Summertime response of ozone and fine particulate matter to mixing layer meteorology over the North China Plain

Jiaqi Wang[1], Jian Gao[1], Fei Che[1], Xin Yang[1], Yuanqin Yang[2], Lei Liu[2], Yan Xiang[3], Haisheng Li[1]

[1]State Key Laboratory of Environmental Criteria and Risk Assessment, Chinese Research Academy of Environmental Sciences, Beijing 100012, China

[2]State Key Laboratory of Severe Weather and Key Laboratory for Atmospheric Chemistry of CMA, Chinese Academy of Meteorological Sciences, Beijing 100081, China

[3]Institutes of Physical Science and Information Technology, Anhui University, Hefei, China

Correspondence to: Jian Gao (gaojian@craes.org.cn), Haisheng Li (lihs@craes.org.cn)

Abstract. Measurements of surface ozone (O_3), $PM_{2.5}$ and its major secondary components (SO_4^{2-}, NO_3^-, NH_4^+, and OC), mixing layer height (MLH) and other meteorological parameters were made in the North China Plain (NCP) during the warm season (June–July) in 2021. The observation results showed that the summertime regional MDA8 O_3 initially increased and reached the maximum value (195.88 μg m^{-3}) when the MLH ranged from approximately 900 to 1800 m, after which the concentration of O_3 decreased with further increase in MLH. Interestingly, synchronous increases in $PM_{2.5}$ concentration along with the development of the mixing layer (MLH < 1200 m) were observed, and the positive response of $PM_{2.5}$ to MLH was significantly associated with the increase in SO_4^{2-} and OC. It was found that this increasing trend of $PM_{2.5}$ with elevated MLH was driven not only by the wet deposition process but also by the enhanced secondary chemical formation, which was related to appropriate meteorological conditions (50 % < RH < 70 %) and increased availability of atmospheric oxidants. Air temperature played a minor role in the change characteristics of $PM_{2.5}$ concentration, but greatly controlled the different change characteristics of SO_4^{2-} and NO_3^-. The concentrations of $PM_{2.5}$, its major secondary components, and SOR and NOR increased synchronously with elevated MDA8 O_3 concentrations, and the initial increase in $PM_{2.5}$ along with increased MLH corresponded well with that of MDA8 O_3. We highlight that the correlation between MLH and secondary air pollutants should be treated with care in hot weather, and the superposition-composite effects of $PM_{2.5}$ and O_3 along with the evolution of mixing layer should be considered when developing $PM_{2.5}$-O_3 coordinated control

30 strategies.
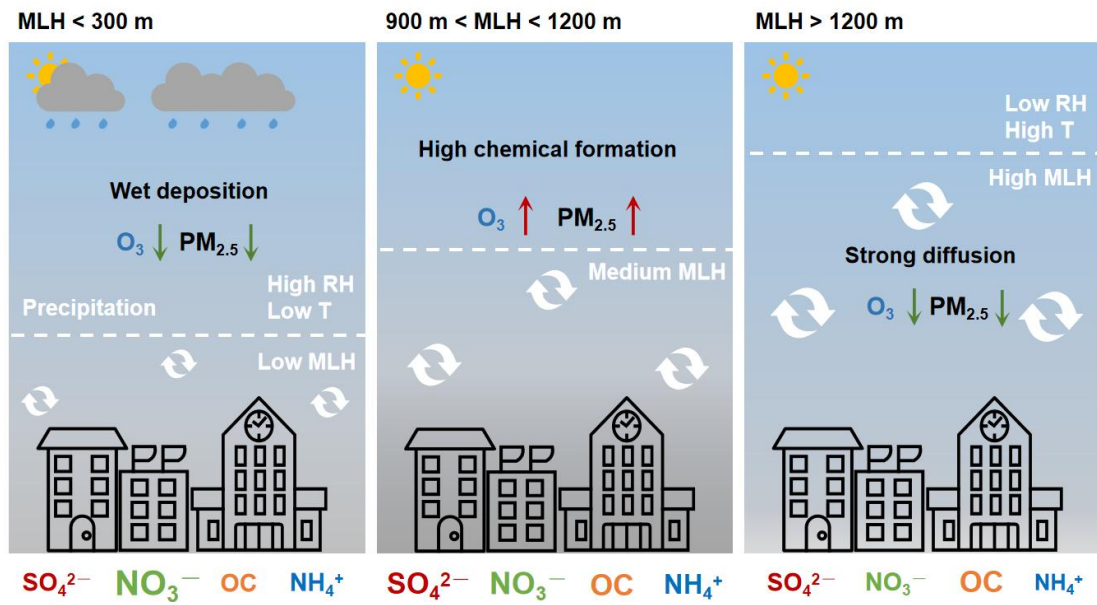
1 Introduction

Surface ozone (O_3) and $PM_{2.5}$ (atmospheric fine particles with an aerodynamic diameter of less than 2.5 μm) are important air pollutants in the atmosphere and have aroused a lot of attention from the public due to their adverse health impacts (Jiang et al., 2018; Cohen et al., 2017; Gao and Ji, 2018). Even though stringent clean air actions have been implemented in China during the past decade, high concentrations of O_3 and/or $PM_{2.5}$ exceeding national air quality standards, still occurred during the warm season, especially in the North China Plain (NCP), the economic centre of China (Dai et al., 2023). O_3 is a secondary pollutant that originates from the photochemical oxidation of volatile organic compounds (VOC) and carbon monoxide (CO) in the presence of nitrogen oxides (NO_X). The level of $PM_{2.5}$ is mainly determined by pollutant emissions and secondary formation from gaseous precursors. In addition to air pollutant emissions, meteorological conditions play critical roles in the formation of $PM_{2.5}$ and O_3 (Miao et al., 2021). The mixing layer height (MLH), which influences vertical mixing within the pollution mixing layer and determines the dilution of pollutants emitted near the ground (Haman et al., 2014; Zhu et al., 2018; Lou et al., 2019), often serves as a critical physical parameter in atmospheric environmental evaluation. Elucidating the association of MLH with surface O_3 and $PM_{2.5}$ is fundamental for the development of $PM_{2.5}$-O_3 coordinated control strategies.

The response of air pollution to the MLH is variable and complicated (Miao et al., 2021). In previous studies, it was often assumed that the narrowing of the mixing layer resulted in the accumulation of pollutants near the ground and the increase in MLH was expected to reduce $PM_{2.5}$ concentration due to dilution (Murthy et al., 2020; Du et al., 2013). However, the relationship between mixing layer structure and $PM_{2.5}$ concentration depends on the site, observation period, and the properties of MLH retrievals (Geiß et al., 2017; Lu et al., 2019). Although the link between $PM_{2.5}$ concentration and MLH has been investigated in many studies, most observations were conducted in winter conditions and comparatively few in hot weather. Interestingly, in some cities, such as Delhi (Murthy et al., 2020) and Shanghai (Pan et al., 2019; Miao et al., 2021), an increase in $PM_{2.5}$ was observed when the MLH increased during summer. As for O_3, the relationship between the changes in the MLH and O_3 concentrations is very complex. Both increase or decrease of O_3 has been observed corresponded to the growth of MLH. Generally, the O_3 concentration decrease with an increase in MLH owing to dilution. However, an increase in the MLH generally promotes the downward mixing of

62 upper air containing higher O_3 (Ma et al., 2021; Haman et al., 2014; Xu et al., 2018). In addition, the

63 meteorological conditions along with the changes of MLH can influence O_3 concentrations through

64 effecting O_3 gaseous precursors or production rates (Porter and Heald, 2019; Zhang et al., 2022). The

65 combined effects of these processes ultimately determine whether the concentration of O_3 decreases or

66 increases.

67 Other meteorological variables in the mixing layer were also found to significantly affect $PM_{2.5}$

68 and O_3 concentrations. Poor air quality in the NCP was closely associated with near-surface southerly

69 winds and warm stagnant conditions during summer (Zhang et al., 2015a). The increase in $PM_{2.5}$

70 concentration often coincided with high relative humidity (RH) conditions (Liu et al., 2017b), which

71 was beneficial to liquid-phase heterogeneous reactions and fine particle hygroscopic growth (Seinfeld

72 and Pandis, 2006; Wang et al., 2016; Zhang et al., 2015b). Temperature was essential to secondary

73 chemical reaction (Dawson et al., 2007). The increase in temperature not only promoted chemical

74 reaction rates, but also stimulated the evaporation of semi-volatile aerosol components, such as nitrate

75 (Wen et al., 2018). As for O_3, elevated concentrations generally occurred on days with strong sunlight

76 and low wind speeds, which favoured photochemical production and the accumulation of O_3 and its

77 precursors. Several studies have shown that O_3 was significantly positively correlated with temperature,

78 but negatively correlated with RH (Li et al., 2021; Hou and Wu, 2016; Steiner et al., 2010).

79 In recent years, long-term $PM_{2.5}$ composition measurements in the NCP have revealed an increase

80 in the contributions of secondary species, e.g., sulfate (SO_4^{2-}), nitrate (NO_3^-), ammonium (NH_4^+), and

81 organic matter (OM) (Cheng et al., 2019; Wang et al., 2022b). As air quality improved ($PM_{2.5}$< 50

82 $\mu g\, m^{-3}$), the correlation between O_3 and $PM_{2.5}$ tended to change from negative to positive in China

83 (Chu et al., 2020). One possible reason is that when the $PM_{2.5}$ concentration is low, $PM_{2.5}$ does not

84 reduce actinic flux and HO_2 radical significantly. On the other hand, $PM_{2.5}$ and O_3 tend to be positively

85 correlated, possibly due to their common precursors, such as VOCs and NOx, and their simultaneous

86 generation in photochemical reactions. In addition, the generation of O_3 enhances the atmospheric

87 oxidation capacity and catalyzes the generation of the secondary $PM_{2.5}$ (Cheng et al., 2019; Kang et al.,

88 2021; Wu et al., 2022). Although some studies have discussed the correlations between MLH and some

89 secondary pollutants, the understanding of the interaction between O_3 and $PM_{2.5}$ (including its major

90 components) along with the evolution of the mixing layer during warm season, remained poor, owing

91 to the limited observations of $PM_{2.5}$ chemical species involved. Regional-scale observation can

92 represent the variation characteristics of an area and avoid spatial heterogeneity between sites.

93 However, to the best of our knowledge, previous observational studies were mostly limited to specific

94 cities. Thus, rather than drawing conclusions based on individual datasets, an analysis of multiple data

95 sources is needed to determine the overall trends.

96   According to the hourly concentrations of $PM_{2.5}$ and MDA8 O_3 in China over the years of

97 2013–2020, the months of June and July can well represent the typical characteristics of O_3–$PM_{2.5}$

98 coordinated pollution during warm season in the NCP (Dai et al., 2023). To enhance the understanding

99 of the linkages between the mixing layer structure and air pollution, in this study, a regional-scale field

100 observation of meteorological factors, O_3, $PM_{2.5}$ concentration and its secondary composition were

101 conducted in the NCP, from 1 June to 31 July, 2021. For the first time, the potential associations

102 between ground-level observed O_3, $PM_{2.5}$ and its dominant components, and mixing layer

103 meteorological conditions in the NCP during summer are presented and discussed.

104 **2 Data and methods**

105 **2.1 Measurements**
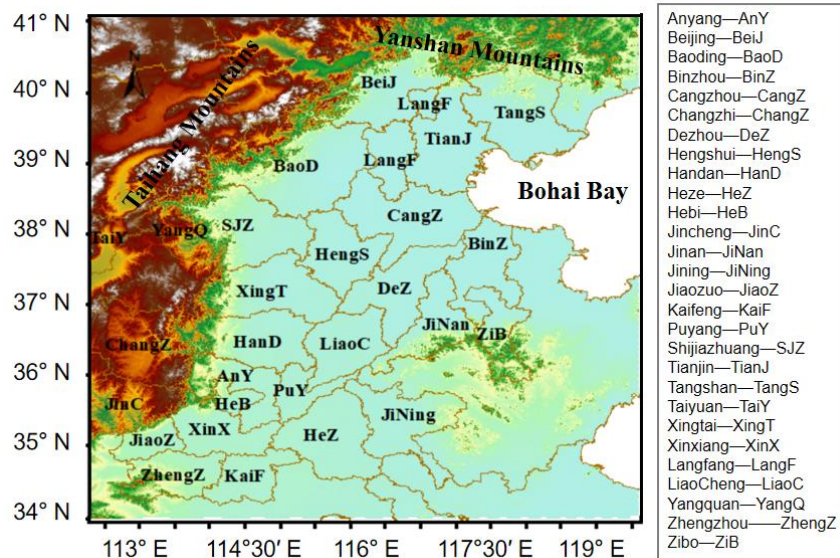
106

107 **Figure 1.** Location of monitoring stations in the North China Plain.

108   Observations were made in the NCP from 1 June to 31 July 2021. Air pollution observation

109 stations covered two megacities (BeiJ and TianJ) and 26 surrounding cities. The geographical locations

110 of these stations are shown in Figure 1. The NCP is bordered by the Taihang Mountains to the west, the

111 Yan Mountains to the north, and the Bohai Sea in the east. The hourly concentrations of ground-level

112 O_3, $PM_{2.5}$ and its major components (SO_4^{2-}, NO_3^-, NH_4^+, and organic carbon [OC]), and meteorological

113 variables, including air temperature, relative humidity (RH), wind speed (WS) and direction (WD), and

114 24-h accumulated precipitation, at the sites were obtained from the platform of National Atmospheric

115 Particulate Chemical-Speciation-Network, which is established for improving the understanding of the

116 heavy pollution formation mechanism in the NCP and supporting the decision-making of local

117 governments and state administration. Hourly SO_2, NO_2, O_3, $PM_{2.5}$ and its chemical compositions were

118 recorded in the $PM_{2.5}$ component network, which was selected following the Technical Regulation for

119 Selection of Ambient Air Quality Monitoring Station published by the Ministry of Ecology and

120 Environment of the People's Republic of China (HJ664−2013). The monitoring sites of the $PM_{2.5}$

121 component network were mostly set up within the cities and reflected the average pollution level of

122 each city. Details of the near-ground observation stations of the $PM_{2.5}$ component network were listed

123 in Table S1. Mass concentrations of SO_4^{2-}, NO_3^-, and NH_4^+ in $PM_{2.5}$ were continuously measured at a

124 1-h resolution by MARGA (model ADI 2080) or AIM-IC (URG 9000D) equipped with a $PM_{2.5}$

125 sampling inlet. These two IC-based online instruments have shown good performance through

126 instrument intercomparison studies or comparison to offline filters under clean to moderately polluted

127 conditions (Markovic et al., 2012; Wu and Wang, 2007; Park et al., 2013; Rumsey et al., 2014). OC

128 was measured online by Sunset Semi-Continuous Carbon Analyzer (Sunset Laboratory Inc, USA). The

129 concentration of OM was obtained by multiplying the OC concentration by a factor of 1.6 (Li et al.,

130 2021). $PM_{2.5}$, O_3, NO_2 and SO_2 concentrations were recorded hourly using Thermo Fisher Scientific

131 samplers and analyzers. Detailed descriptions of these online sampling instruments can be found in our

132 previous works (Kong et al., 2018; Liu et al., 2017a; Pang et al., 2020; Wang et al., 2022b). The

133 meteorological variables were recorded in the national meteorological observation stations, and the

134 information of each station was obtained from the public website of the China Meteorological

135 Administration (http://data.cma.cn/data/cdcindex/cid/0b9164954813c573.html). The temporal

136 resolution of air temperature, RH, WS and WD was 1 hour. To avoid the influence of diurnal boundary

137 layer cycles, this study focused on the relationship between the daily mean air pollutants and

138 meteorological factors. The daily mean meteorological factors, $PM_{2.5}$ and its major secondary

139 components were calculated from the hourly data, and the daily O_3 concentration was characterized by

140 the maximum daily 8 h average ozone (MDA8 O_3). Details for the near-ground observation species and

141   the metrics were shown in Table S2.

142   To better demonstrate the overall change characteristics of the regional air pollution and

143   meteorological conditions during the observation period, the occurrence frequency (%), which is the

144   proportion of the cities at each air pollutant or methodology level, was calculated based on the

145   following equation:

146    $\text{Occurrence frequency}_X^{level} = \frac{N_X^{level}}{\text{Total } N_X} \times 100\ \%$ (1)

147   where X means the air pollutants or methodology factors, N_X^{level} represents the number of cities at each

148   X level, and $\text{Total } N_X$ represents the total number of cities.

2.2 The calculation of MLH

150   In recent years, many works have progressed in the atmospheric boundary layer characteristics,

151   and analyzed the impacts of these parameter on air pollution (Haugen et al., 1971; Wang et al., 2014;

152   Zhang et al., 2005). However, the way the boundary layer describes the influences of air pollution is

153   easily duplicated and confused (Niu et al., 2017). For air pollution measurement, one of selected

154   functionalities of parameterization scheme for pollution mixing layer is to judge whether an air mass

155   over a specific locality satisfies the "static and stable" attribute or not. Therefore, in this work, to

156   express the basic physics for diagnosing meteorological conditions, we used the concept of pollution

157   MLH proposed by Wang et al. (2017), which was based on the classical synoptic theory according to

158   the level of the convective condensation layer, and the details of this method can be seen in previous

159   work (Wang and Yang, 2000; Wang et al., 2017).

160   To be specific, we defined the height close to the cloud base as the height of the super-saturation

161   layer (H_SSL). The isoentropic atmospheric process meets the level of the convective condensation

162   layer (LCL) in the supersaturation state, that is, it is very close to the H_SSL. An iterative algorithm

163   was used to work out the H_SSL (Wang and Yang, 2000):

164    $\text{H\_SSL} \approx \text{LCL} = 6.11 \times 10^2 \times \left(\frac{0.622 + 0.622\frac{e_s}{p-e_s}}{0.622\frac{e_s}{p-e_s}} \right),$ (2)

165    $e_s = 6.22 \times \exp{\frac{17.13(T-273.16)}{T-38}},$ (3)

166   where e_s represents the saturated water vapour pressure, and T is the temperature (K). Eq. (2) can be

167   used to calculate the H_SSL which is favourable for pollutant mixing and is represented by (P). Below

168   this height, the atmosphere gets supersaturated, causing the pollution mixing and wetting process in the

169   low altitude to continue, so this height is called the height of pollution mixing layer (MLH). Thus,

170   MLH can be derived in the following expression:

171     $MLH \approx H\_SSL \approx LCL = 6.11 \times 10^2 \times \left(\frac{0.622 + 0.622 \frac{e_s}{p - e_s}}{0.622 \frac{e_s}{p - e_s}} \right),$ (4)

172   According to the relationship between air pressure and height, the units of MLH can be converted to

173   the height (in m) as follows:

174     $\int_{p_0}^{p_z} dp = - \int_0^z \rho_0 g \, dz,$ (5)

175   where z is the height, ρ_0 is the density of gas, p_z and p_0 represent the air pressure in the height of z and

176   0, respectively.

177   Several works have verified the reliability of the results based on this method. Using this method,

178   Wang et al. (2017) well characterized the features of the mixing layer height in highly-sensitive areas

179   of pollution in China. Wang et al. (2022c) also used this method to explore $PM_{2.5}$ and O_3

180   superposition-composite pollution events during spring 2020 in Beijing, China, and the hourly

181   evolution of MLH, O_3, and $PM_{2.5}$ during the observation period was analyzed. In addition, Niu et al.

182   (2017) has applied this method to Beijing, and the results showed that the pollution mixing layer could

183   effectively represent the change characteristics of the haze pollution process. In this work, we applied

184   this method to investigate the impact of MLH on the change characteristics of ozone and fine

185   particulate matter.

186   **3 Results and discussion**

187   **3.1 General characteristics**
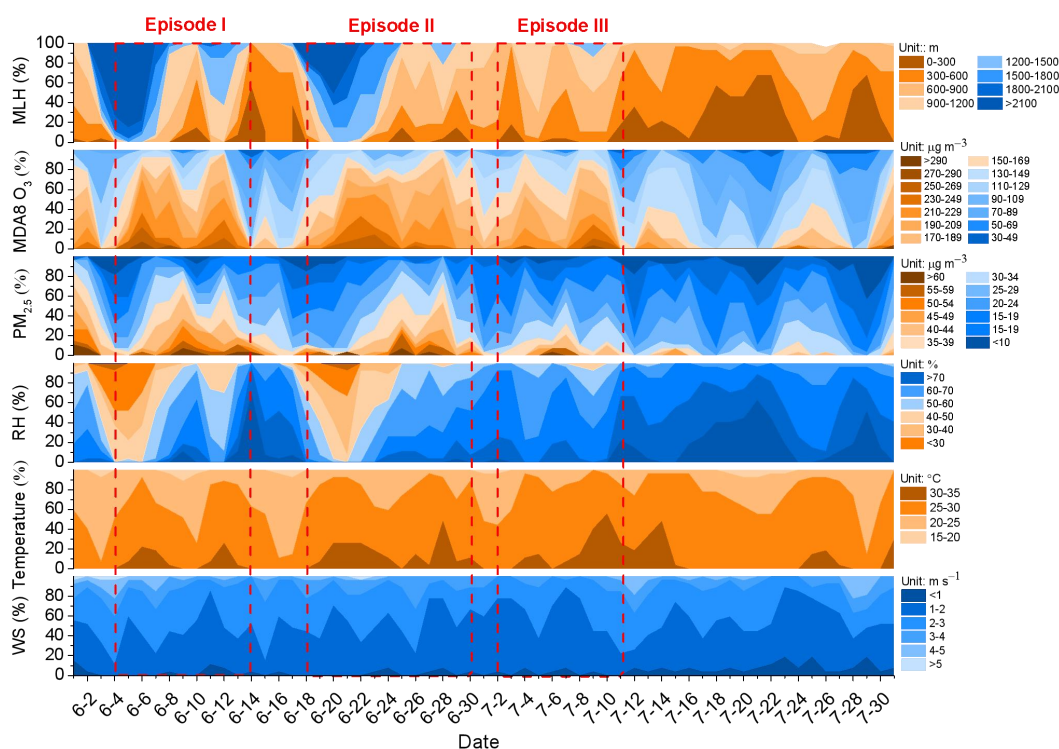
Figure 2. Occurrence frequency (%) of PM$_{2.5}$, MDA8 O$_3$, and meteorological factors under different levels in the NCP from June 1 to July 31, 2021. The color shading represents different categories classified by PM$_{2.5}$, MDA8 O$_3$, and meteorological factors. Boxed areas delineated by red dashes represent three typical PM$_{2.5}$ and O$_3$ co-polluted episodes: June 4–14 (Episode I), June 18–29 (Episode II), and July 2–11 (Episode III), 2021.

The summertime change characteristics of ground-level meteorological factors (MLH, RH, temperature, and WS), MDA8 O$_3$, PM$_{2.5}$ and its major components in the NCP were shown in Figures 2 and S1. The primary atmospheric pollutant in the NCP during the summer was O$_3$, and the concentrations of MDA8 O$_3$ averaged over all sites in the NCP varied from 74.94 to 219.28 μg m^{-3}, with the mean value of 151.72 μg m^{-3} (Table 1). O$_3$ pollution lasted for nearly the entire observation period and was characterized by frequent and long-lasting pollution episodes. The PM$_{2.5}$ concentration was much lower comparing with O$_3$ during the observation period. The mean, maximum, and minimum of the regional daily mean PM$_{2.5}$ concentration was 25.62, 45.62, and 11.32 μg m^{-3}, respectively. NO$_3^-$ was the prominent PM$_{2.5}$ component, with the mean concentration of 7.76 μg m^{-3}. According to the National Ambient Air Quality Standard of China (GB3095-2012), the daily PM$_{2.5}$ averages in "2+26" cities can meet the Level II standard of 75 μg m^{-3}, while exceeding the level I standard (35 μg m^{-3}). As shown in Figure 2, the regional PM$_{2.5}$ pollution processes corresponded well with the increasing processes of MDA8 O$_3$. Here, we define a O$_3$–PM$_{2.5}$ co-polluted episode as a set of

207 continuous days (longer than 4 days) with MDA8 O_3 and daily mean $PM_{2.5}$ (in more than 10 % NCP

208 cities) exceeding 160 and 35 μg m^{-3}, respectively. On the basis of this criterion, three typical O_3–$PM_{2.5}$

209 co-polluted episodes were selected: June 4–14 (Episode I), June 18–29 (Episode II), and July 2–11

210 (Episode III), 2021.

211 During these three typical episodes, the synchronous change characteristics of air pollutants and

212 the mixing layer meteorology were analyzed. In Episode I and II, when MLH was higher than 2100 m,

213 both MDA8 O_3 and $PM_{2.5}$ concentrations were low. Along with the reduction in MLH (from

214 1800–2100 m to 1200–1800 m), regional MDA8 O_3 and $PM_{2.5}$ concentrations both gradually increased.

215 When MLH fell in the range of 1200–1800 m, MDA8 O_3 concentration reached the maximum with

216 approximately 80 % areas having levels greater than 170 μg m^{-3}. With a further decrease in MLH,

217 MDA8 O_3 declined, whereas $PM_{2.5}$ remained stable or continued to increase, when the regional MLH

218 was in the range of 600–1200 m. In Episode III, the MLH in most cities was lower than 1200 m, and

219 the regional MDA8 O_3 and $PM_{2.5}$ pollution conditions were lighter than other episodes, with 80 % of

220 the $PM_{2.5}$ values less than 35 μg m^{-3}. It is interesting to note that the change characteristics of SO_4^{2-} and

221 NO_3^- differed (Figure S1), and the regional peaks of these two components were inconsistent,

222 especially in Episode II. With the evolution of MLH, NO_3^- climbed up and peaked on June 24 when

223 regional MLH lower that 900 m, and SO_4^{2-} reached the maximum on June 28 when MLH was

224 approximately 900–1500 m. This may be related to other synchronized mixing layer meteorological

225 factors, such as RH and temperature. For example, the evolution of the mixing layer is often

226 accompanied by changes in temperature. The increase in temperature can promote the chemical

227 formation rate of these secondary components, but also stimulate the volatilization of NO_3^- to gaseous

228 state (HNO_3) , which leads to the decrease in NO_3^- concentration. Further analysis of the responses of

229 O_3, $PM_{2.5}$ and its secondary components to different mixing layer meteorological factors is presented in

230 the following sections.

231 Table 1. General information on O_3–$PM_{2.5}$ co-polluted episodes from June 1 to July 31, 2021.

	Episode I			Episode II			Episode III			Summer		
	Ave.	Min	Max	Ave.	Min	Max	Ave.	Min	Max	Ave.	Min	Max
Gaseous pollutants (μg m^{-3})												
MDA8 O_3	170.80	85.62	219.28	180.65	142.10	204.15	168.70	111.79	199.39	151.72	74.94	219.28
SO_2	10.01	6.48	14.44	9.09	6.11	12.48	6.75	5.72	8.00	7.59	4.79	14.44

NO₂	24.61	16.26	31.81	22.89	14.11	32.15	17.66	13.12	21.00	19.31	10.90	32.15

PM₂.₅ and its major components (μg m⁻³)

PM₂.₅	30.55	15.74	42.67	28.33	17.22	42.52	25.05	20.84	31.75	25.62	11.32	45.62
NO₃⁻	8.74	2.16	16.44	8.29	2.85	18.00	7.67	5.87	13.44	7.76	2.16	18.24
SO₄²⁻	7.22	2.81	10.25	7.32	4.02	12.15	7.12	5.48	8.92	7.04	2.81	12.15
NH₄⁺	5.51	1.42	9.34	5.52	2.27	9.29	5.38	4.46	8.21	5.30	1.42	9.88
OC	5.11	2.74	6.60	4.71	3.25	6.75	4.11	2.90	5.30	4.32	2.69	6.75

Meteorological variables

MLH (m)	1342.73	305.93	2423.42	1190.36	626.51	2127.31	740.86	460.91	950.10	855.99	305.93	2423.42
T (°C)	26.24	23.86	28.91	27.41	25.53	28.76	27.58	24.85	30.14	26.69	22.48	30.14
RH (%)	57.01	32.78	90.54	56.90	37.04	70.60	71.45	64.64	80.38	68.70	32.78	90.54

3.2 Evolution of ozone with mixing layer meteorology
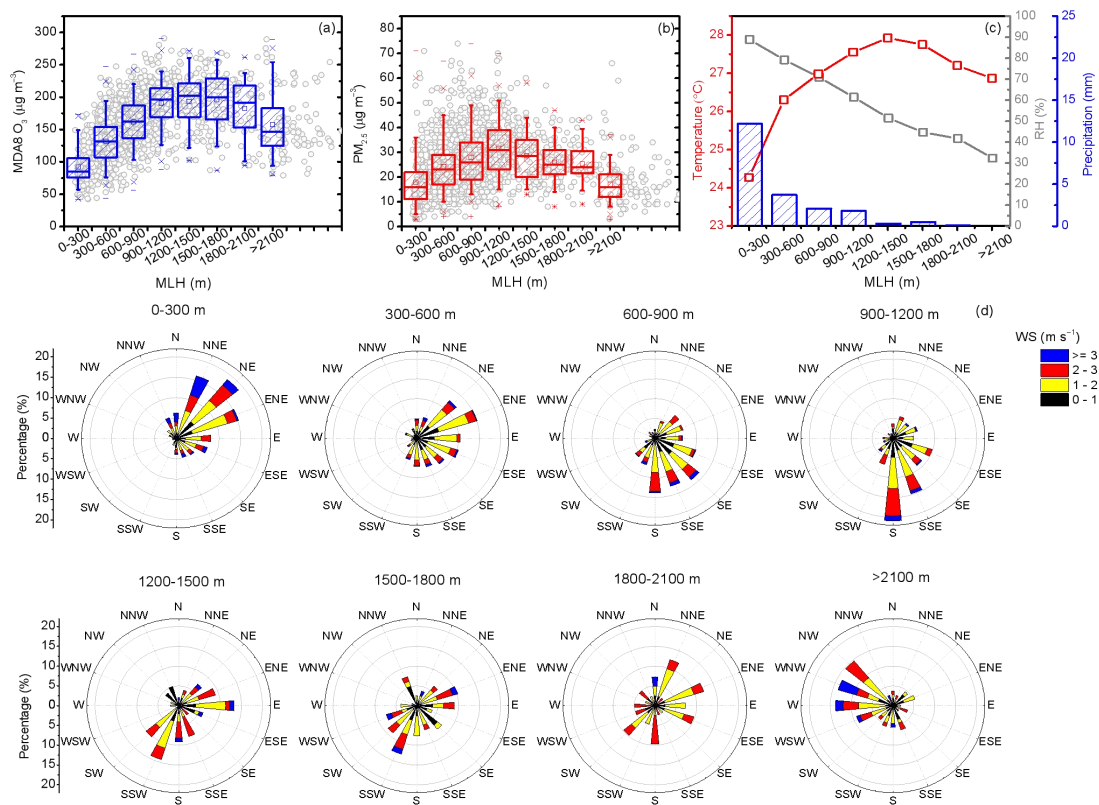
Figure 3. Variation characteristics of (a) MDA8 O₃, (b) PM₂.₅, (c) temperature, RH, 24-h precipitation, and (d) WS and WD in different MLH conditions. Box plots in (a) and (b) show the inter quartile range (the distance between the bottom and the top of the box), median (the band inside the box), and 95 % confidence interval (whiskers above and below the box) of the data.

To quantify the effect of MLH on near-ground O₃ concentrations, relationships between MLH and MDA8 O₃ were analyzed (Figure 3a). A data binning method was used to remove the expected

239 day-to-day atmospheric variability from the sampling uncertainty (Dian et al., 2010), which has been

240 applied in other studies (Lou et al., 2019). The MLH was grouped into 8 classes of 300 m width: 0–300,

241 300–600, 600–900, 900–1200, 1200–1500, 1500–1800, 1800–2100 and > 2100 m. It was found that

242 MDA8 O_3 concentration dramatically increased when MLH fell in the range of 0–900 m, and leveled

243 off when MLH at approximately 900–1800 m, with the maximum MDA8 O_3 of 195.88±42.76 μg m^{-3},

244 after which the concentration began to decrease with further development of MLH. This nonlinear

245 relationship between MDA8 O_3 and MLH was is consistent with the results reported by Zhao et al.

246 (2019), which found that the O_3 concentration was highest at medium boundary layer heights

247 (1200–1500 m) during summertime in Shijiazhuang, China.

248   The relationship observed between MDA8 O_3 and MLH is complex. Previous studies have shown

249 that a higher MLH can lead to the mixing of near-surface air with the O_3 rich air aloft, resulting in

250 enhanced surface O_3 concentrations (Reddy et al., 2012). Concurrently, the evolution of the mixing

251 layer was strongly associated with the changes in other meteorological conditions, such as air

252 temperature, RH and precipitation, which can also affect the O_3 concentration (Haman et al., 2014).

253 The combined effects of these processes ultimately determine whether ground-level O_3 increases along

254 the evolution of the mixing layer. The increase in the MLH often coincides with higher air

255 temperature, lower RH, and less precipitation (Figure 3c), and this combination of factors is more

256 conducive to O_3 production (Ma et al., 2021; Xu et al., 2018). As shown in Figure 4a–c, as the MLH

257 remained constant, the MDA8 O_3 concentration climbed up with the increase in air temperature but

258 decrease in RH and precipitation levels. Possible reasons for these results are: (1) the increase in RH

259 contributes to the depletion of O_3, and leads to weakened O_3 related photochemical reaction (Ma et al.,

260 2021; Yu, 2019); (2) due to higher RH or rain fall, gaseous precursors and O_3 are washed out from the

261 atmosphere trough wet deposition (Reddy et al., 2012); and (3) the rise of temperature accelerates the

262 emission rate of gaseous precursors, such as biogenic VOCs and soil NO_X (Dang et al., 2021; Porter

263 and Heald, 2019), and also stimulates the photochemical reaction rate in the generation of O_3 (Ma et al.,

264 2021). Wind fields also alter surface O_3 concentrations by transporting O_3 or its precursors into and out

265 of the region (Ma et al., 2021). As shown in Figure S2, during the entire campaign, the NCP was

266 dominated by winds from the northeast and south (45°−225°). Because more than 75 % WD were in

267 the range of 45°−225°, the WD was classified into four categories: 45°−90°, 90°−135°, 135°−180°, and

268 180°−225°. As shown in Figure 3d, along with the evolution of the mixing layer, the WD gradually

269   changed from the northeast (MLH=0−600 m) to the southeast (MLH=600−900 m) and south

270   (MLH=900−1200 m). Southerly winds can transport the gaseous pollutants or O_3 from the southern

271   part of the plain area to the northern part, and the Taihang mountains may block pollutant transport,

272   leading to pollutant accumulation at the foot of the Taihang Mountains. It should be noted that the

273   concentration of MDA8 O_3 was higher when the plain was dominated by southerlies (180°−225°) when

274   MLH was lower than 1200 m (Figure 4e). Generally, WS can affect the diffusion of air pollutants.

275   Owing to the limited dilution and dispersion effects of weak winds, the MDA8 O_3 concentrations at low

276   wind speed (0−1 m s^{-1}) were relatively higher than those of the other WS conditions (Figure 4d) .
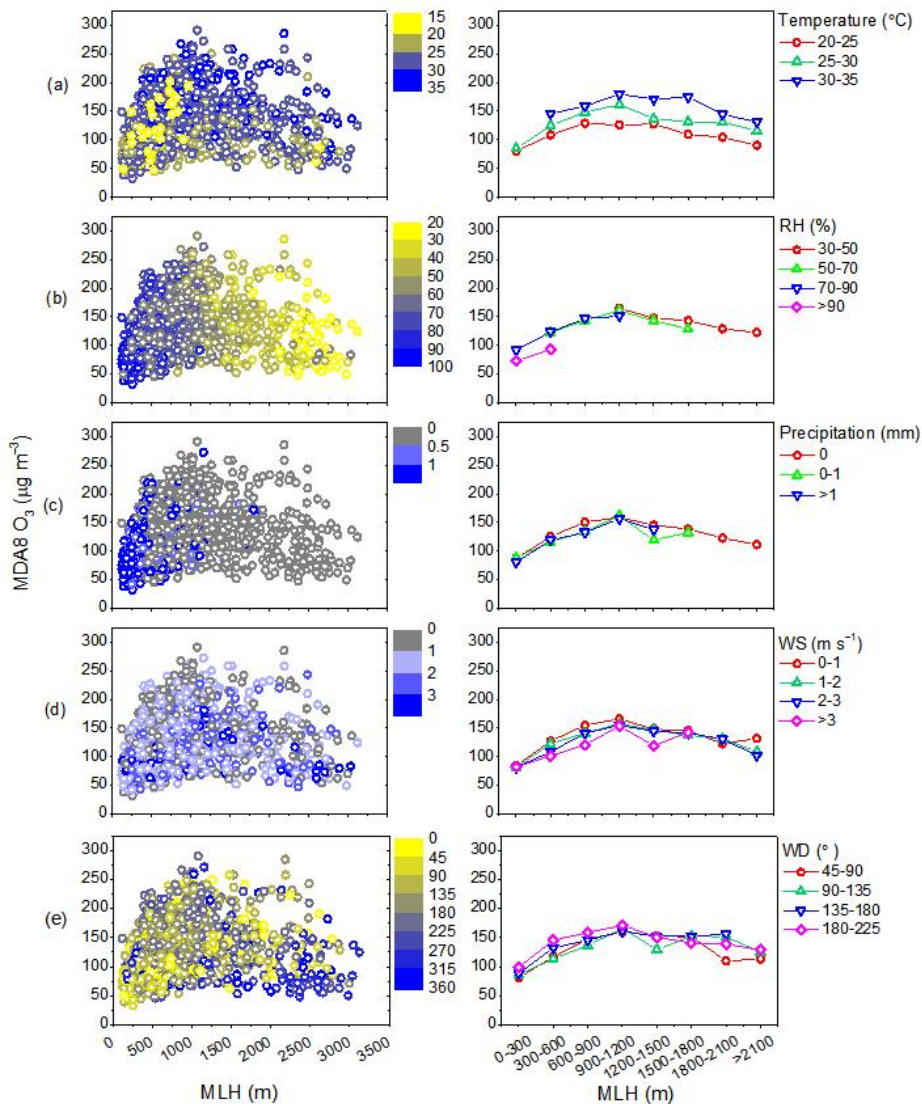
277

278   **Figure 4.** Distribution characteristics of the MDA8 O_3 concentrations with the evolution of MLH under

279   different (a) temperature, (b) RH, (c) precipitation, (d) WS, and (e) WD conditions.

280   **3.3 Evolution of PM$_{2.5}$ and its secondary compositions with mixing layer meteorology**

281   The concentration distribution of surface $PM_{2.5}$ in different MLH bins was shown in Figure 3b.

282   Interestingly, $PM_{2.5}$ showed a similar change profile as MDA8 O_3, which initially increased and then

283   declined with the growth of MLH. $PM_{2.5}$ concentration reached the maximum of 31.65 μg m^{-3} when

284   MLH fell in the range of 900–1200 m, and the concentration has increased by 1.51 μg m^{-3} through the

285   rise phase for the variation of 100 m MLH. This phenomenon differs from the results obtained in the

286   cold season (Pan et al., 2019; Du et al., 2013; Murthy et al., 2020). It has been suggested that the

287   narrowing of the mixing layer compressed air pollutants into a shallow layer, resulting in elevated

288   pollution levels; thus, MLH has been illustrated as the key factor that aggravated the haze events in

289   large cities of China in winter. However, the response of $PM_{2.5}$ concentration to MLH is not only

290   determined by the vertical stratification of the mixing layer, but also by local sources, secondary

291   chemical formation, wet deposition, and the wind field (Lu et al., 2019; Geiß et al., 2017; Pan et al.,

292   2019; Miao et al., 2021; Lou et al., 2019). It should be noted that in this work, there were still some

293   extremely high $PM_{2.5}$ values under low MLH conditions, as shown in Figure 3b. This phenomenon will

294   be discussed in the following part when exploring the effect of precipitation.
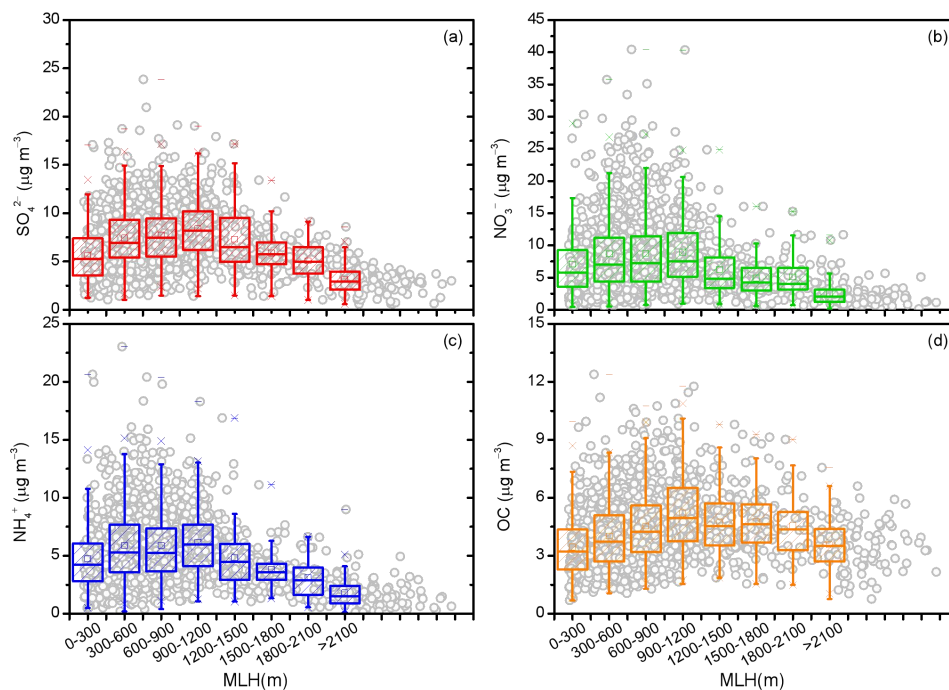
295

296   Figure 5. Variation characteristics of (a) SO_4^{2-}, (b) NO_3^{-}, (c) NH_4^{+}, and (d) OC in different MLH

297   conditions. Box plots show the inter quartile range (the distance between the bottom and the top of the

298   box), median (the band inside the box), and 95 % confidence interval (whiskers above and below the

299   box) of the data.

300
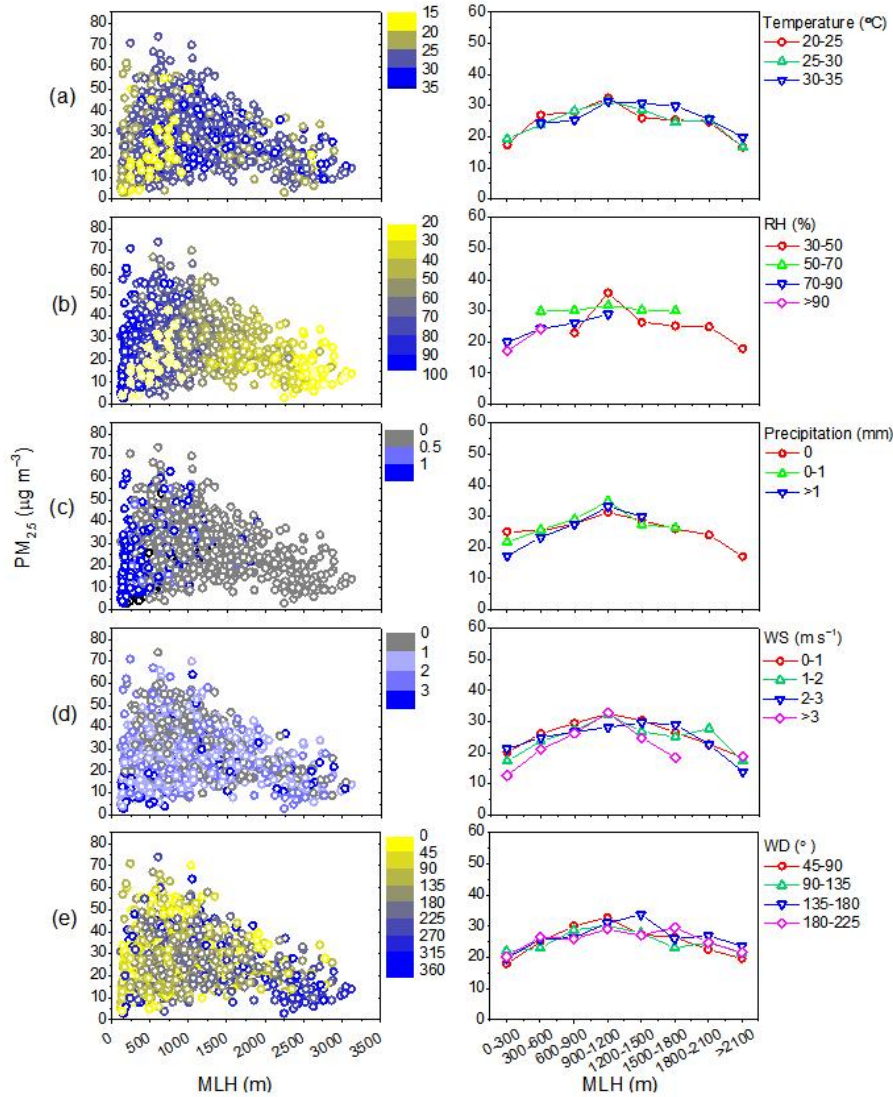
Figure 6. Distribution characteristics of the PM$_{2.5}$ concentrations with the evolution of MLH under

different (a) temperature, (b) RH, (c) precipitation, (d) WS, and (e) WD conditions.

The response of PM$_{2.5}$ concentrations to mixing layer structure was the net effect of the changes in

PM$_{2.5}$ major chemical components, such as SO$_4^{2-}$, NO$_3^-$, NH$_4^+$, and OC. The changes in the major

components of PM$_{2.5}$ due to the evolution of the mixing layer were shown in Figure 5. All the

secondary components showed increasing trends when MLH was lower than 1200 m, with SO$_4^{2-}$ and

OC showing the highest increment, followed by NO$_3^-$ and NH$_4^+$. When MLH changed from 300−600

m to 900−1200 m, the increment was not significant for NO$_3^-$ and NH$_4^+$. As NH$_3$ was generally

abundantly supplied in the NCP, the formation of NH$_4^+$ was predominantly controlled by the reaction of

ammonia with sulfate and nitrate aerosols, and the changes in NH$_4^+$ were a consequence of the changes

in SO$_4^{2-}$ and NO$_3^-$ (Chow et al., 2022). When MLH<1200 m, the mass fraction of NO$_3^-$ was higher

than SO$_4^{2-}$ in PM$_{2.5}$ (Figure S3), and the change characteristics of NH$_4^+$ along with the evolution of

313   mixing layer were consistent with that of NO_3^-. The mass ratio of SO_4^{2-} to NO_3^- gradually increased

314   along with the development of mixing layer. When MLH was higher than 1200m, SO_4^{2-} surpassed

315   NO_3^- and became the dominant $PM_{2.5}$ component. The difference in the relationships between these

316   aerosol species and MLH reflected the intrinsic complexity mechanisms of $PM_{2.5}$ formation, which

317   were probably related to other meteorological parameters, such as temperature, RH, precipitation, WS,

318   and WD. To understand how the other meteorological factors impacted the relationship between MLH

319   and $PM_{2.5}$, we analyzed the statistics on the concentration distribution of $PM_{2.5}$ and its dominant

320   components with the increase in MLH under different RH, temperature, precipitation, WS, and WD

321   conditions (Figures 6 and 7).

322   Temperature is not only essential for the secondary chemical reaction of trace gases but also for

323   the gas–particle partitioning of volatile $PM_{2.5}$ species. The response of $PM_{2.5}$ and its dominant

324   components to MLH, followed similar change characteristics under different temperature conditions,

325   all increasing with the development of the mixing layer when MLH was lower than 1200 m. The

326   response of $PM_{2.5}$ to temperature was largely the result of opposite changes in NO_3^- and SO_4^{2-}

327   concentrations with a smaller role played by organics (Figure 7). Specifically, as MLH kept constant,

328   SO_4^{2-} concentration climbed up with increasing temperature level, while the concentration of NO_3^-

329   declined when temperature kept going up. Higher temperature may promote faster oxidation of SO_2 to

330   SO_4^{2-}, resulting in a significant increase in SO_4^{2-} concentrations. Unlike SO_4^{2-}, which predominantly

331   exists in the particle phase, NO_3^- could be either presented as nitric acid (HNO_3) in the gas phase or as

332   ammonium nitrate (NH_4NO_3) in the particle phase (Chow et al., 2022). Temperature strongly

333   influenced the partitioning of nitrate between the gas and particle phases. Higher temperature prompts

334   the partitioning of nitrate to HNO_3; thus, nitrate tends to exit in the gas phase, resulting in a significant

335   decrease in NO_3^- and NH_4^+ concentrations.

336   The response of $PM_{2.5}$ and its dominant components to the evolution of the mixing layer was more

337   sensitive to RH, and the distinct distribution characteristics under different RH ranges were shown in

338   Figures 6 (b) and 7 (b). When MLH fell in the range of 300–900 m, the concentration of $PM_{2.5}$ (Figure

339   6b) and its major components (Figure 7b) mostly decreased with RH rising from 50–70 % to 70–90 %.

340   Previous studies have shown that when RH higher than 60%, local humidity-related physicochemical

341   processes play important roles in transforming the gases into aerosols (Wang et al., 2022d; Liu et al.,

342   2020). We considered that the RH range from 50% to 70% was more beneficial for the aqueous

343   chemical production of major $PM_{2.5}$ components, thus leading to the increase in $PM_{2.5}$ concentration. It

344   is worth noting that when MLH fell in the range of 0–300 m, with RH increasing from 70–90 % to >

345   90 %, the concentration of $PM_{2.5}$ (Figure 6b) and its major components (Figure 7b) severely decreased,

346   which was probably related to the fast hygroscopic growth and enhanced wet deposition processes.

347   All aerosol species have wet deposition as a major sink; therefore, precipitation is expected to

348   have significant effects on $PM_{2.5}$ concentrations. As shown in Figure 6(c), changes in the

349   concentrations of $PM_{2.5}$ were sensitive to rain events. When the MLH fell in the range of 0–300 m, the

350   concentration of $PM_{2.5}$ significantly decreased during the rainfall period. Interestingly, when no rainfall

351   occurred, even though the $PM_{2.5}$ concentration kept stable under low MLH conditions, its response of

352     $PM_{2.5}$ concentrations to MLH followed an upward trend as the MLH increased from 300–600 to

353   900–1200 m. As for specific aerosol species (Figure 7c), NO_3^- and NH_4^+ concentration showed two

354   prominent peaks, with one in the range of 0–300 m, and the other in 900–1200 m. Under low MLH

355   condition, the concentrations of NO_3^- and NH_4^+ were high, with NO_3^- as the dominant species in $PM_{2.5}$

356   (Figure 8b). With the growth of MLH, NO_3^- and NH_4^+ initially decreased, but turned to increase again

357   when MLH fell in the range of 900–1200 m. As for SO_4^{2-} and OC, the concentrations increased with

358   the elevation of MLH and has exceeded that of NO_3^- when MLH was higher than 1200 m. As shown in

359   Figure 8 (a), low mixing layer was generally accompanied by cloudy and rainy conditions during

360   summer in the NCP in 2021, and only a small fraction of days without rainfall were captured during

361   this period. Therefore, despite some high $PM_{2.5}$ or major aerosol species values have been witnessed

362   under low MLH conditions, the overall trend in Figure 3 (b) was still upward along with the growth of

363   the mixing layer (MLH < 1200 m). The increase in $PM_{2.5}$ and its major chemical components under

364   medium MLH conditions was not only associated with the weaker particle removal process by

365   precipitation, but also related to the enhancement of secondary aerosol formation due to the appropriate

366   chemical reaction environment.

367   WS can represent the atmospheric dissipation potential in the horizontal directions (Zhu et al.,

368   2018). Low WS generally suggests weak pressure gradients and potentially more favourable

369   meteorological conditions for $PM_{2.5}$ enhancement (Ma et al., 2021). As expected, the concentrations of

370     $PM_{2.5}$ (Figure 6d) and its aerosol species (Figure 7d) gradually decreased with increasing WS. The

371   response of these air pollutants to the MLH followed similar upward trends under different WS

372   conditions (MLH < 1200 m). Compared with O_3, the impact of WD along with the increase in MLH

373 seems different for PM$_{2.5}$ and its dominant components. When the MLH fell in the range of 600−1200

374 m, the NCP was dominated by southeast or southern winds (Figure 3d). However, when southeast or

375 south winds prevailed, the corresponding PM$_{2.5}$ and its dominant component concentrations were

376 comparable or even lower than in other WD situations (Figures 6e and 7e). This indicated that regional

377 transport was not the dominant factor leading to the elevation of PM$_{2.5}$ and its aerosol species along

378 with the evolution of the mixing layer (MLH < 1200 m).
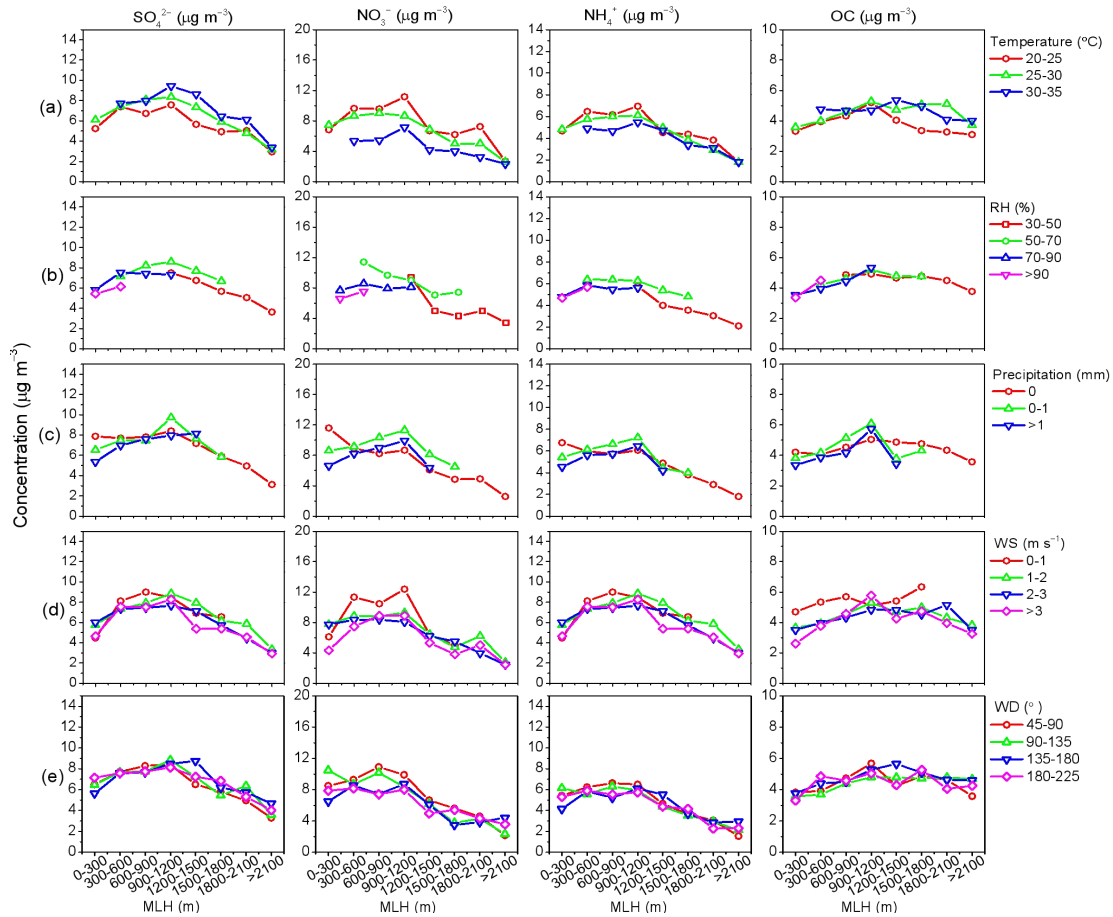
379 **Figure 7.** Distribution characteristics of NO$_3^-$, SO$_4^{2-}$, NH$_4^+$, and OC concentrations with the evolution

380 of MLH under different conditions: (a) temperature, (b) RH, (c) precipitation, (d) WS, and (e) WD.
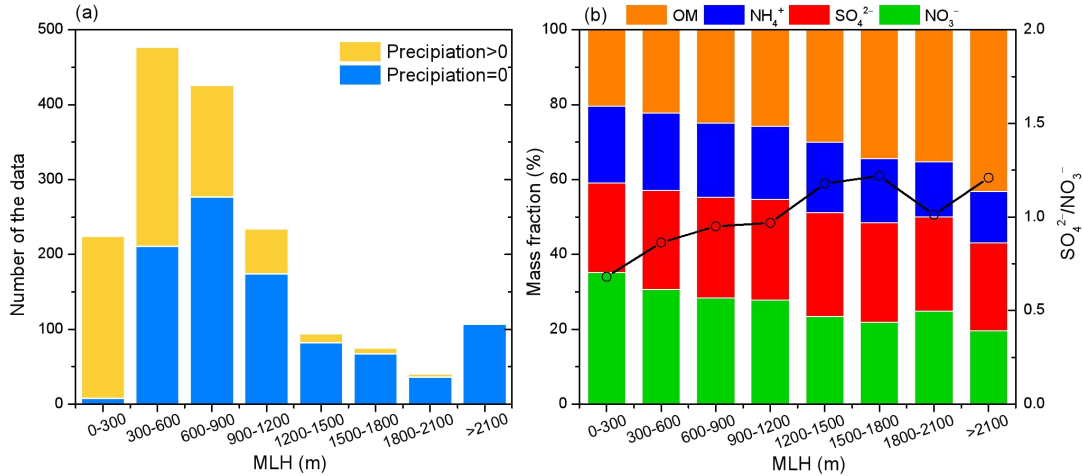
Figure 8. (a) Number distributions of the data when the daily precipitation larger than 0 mm or equal to 0 mm along with the evolution of MLH. (b) Mass fractions of major $PM_{2.5}$ components and the mass ratio of SO_4^{2-} to NO_3^- along with the evolution of MLH when the daily precipitation equal to 0 mm.

3.4 Superposition-composite effects of $PM_{2.5}$ and O_3 with the evolution of mixing layer

3.4.1 A case study of the typical $PM_{2.5}$-O_3 co-polluted episode

Previous results have indicated that MDA8 O_3 and $PM_{2.5}$ concentrations were closely related to the evolution of the MLH. The increasing trend of $PM_{2.5}$ concentration with the development of mixing layer under medium MLH condition indicated that the evolution of the mixing layer was not a simple physical dilution process, and its influence on the enhanced secondary photochemical formation should also be considered. We illustrated the relationship between the mixing layer and pollutant levels in Figures 9 and 10, showing a typical $PM_{2.5}$-O_3 co-polluted episode (Episode II) during June 18−29, 2021. On June 18−20, the MLH gradually increased from 600−1200 m to 1500−3000 m in the southern and eastern parts of the NCP, and the $PM_{2.5}$ and MDA8 O_3 concentrations concurrently increased and showed similar spatial distributions. The WS dropped significantly on 20 June, and the value was lower than 1 m s^{-1} in most cities. On 21−23 June, the MLH began to decrease from 1500−3000 m to 1200−1800 m, $PM_{2.5}$ and MDA8 O_3 concentrations further increased, and the areas of high $PM_{2.5}$ concentrations also coincided well with those of MDA8 O_3 concentrations. During 24−25 June, the MLH continued to decrease, with some values even lower than 300 m. The MLH for the areas with high MDA8 O_3 was in the range of 900−1500 m. Interestingly, the synchronized spatial change characteristics of $PM_{2.5}$ and MDA8 O_3 were consistent when MLH fell in the range of 900−1200 m, but inconsistent when MLH was lower than 600 m. Significant rise of $PM_{2.5}$ concentration was observed in

403   some cities with MLH lower than 300 m. It is noted that the dominant chemical composition of $PM_{2.5}$

404   in these areas was NO_3^-. On 28 June, the rise in MLH was observed in the central and the southern part

405   in the NCP, and a surge in MDA8 O_3 and $PM_{2.5}$ concentrations occurred: with 160−220 and 40−50 μg

406   m^{-3} respectively. In general, most cities were dominated by weak winds from the east and southeast,

407   which favoured the formation of secondary pollutants from gaseous precursors transported from the

408   southeast part and promoted the accumulation of air pollutants.

409   To better understand this $PM_{2.5}$-O_3 co-polluted event, here we classified the observations during

410   this typical event into four categories: O_3 polluted days (O_3PD; MDA8 O_3 concentration $> 160 \, \mu g \, m^{-3}$

411   and $PM_{2.5} < 35 \, \mu g \, m^{-3}$), $PM_{2.5}$ polluted days ($PM_{2.5}$PD; MDA8 O_3 concentration $< 160 \, \mu g \, m^{-3}$ and

412    $PM_{2.5} > 35 \, \mu g \, m^{-3}$), O_3–$PM_{2.5}$ co-pollution days (O_3–$PM_{2.5}$CPD; MDA8 O_3 concentration $> 160 \, \mu g \, m^{-3}$

413   and $PM_{2.5} > 35 \, \mu g \, m^{-3}$), and non-polluted days (NPD; MDA8 $O_3 < 80 \, \mu g \, m^{-3}$ and $PM_{2.5} < 35 \, \mu g \, m^{-3}$).

414   The meteorological and chemical characteristics of the O_3–$PM_{2.5}$ CPD, O_3PD, $PM_{2.5}$ PD, and NPD were

415   presented in Figure 11. The results indicated that the values of MLH on O_3–$PM_{2.5}$CPD were between

416   those on O_3PD and $PM_{2.5}$PD at approximately 900 m. On O_3–$PM_{2.5}$CPD, the oxidation ratio of sulfate

417   (SOR, the molar ratio of sulfate to the sum of sulfate and SO_2) and oxidation ratio of nitrate (NOR, the

418   molar ratio of nitrate to the sum of nitrate and NO_2) were the highest, with values of 0.44 and 0.33,

419   respectively, which indicated the strong secondary formation of SO_4^{2-} and NO_3^- promoted by high O_3

420   concentration. The $PM_{2.5}$PD occurred when MLH was lower than 650 m, and the percentage of NO_3^-

421   was the highest on $PM_{2.5}$PD. The rise in $PM_{2.5}$ in some cities under low MLH conditions, may be

422   attributed to three mechanisms. The first is the accumulation effect due to unfavourable diffusion

423   conditions when MLH decreased. Secondly, these cities experienced little rain, and the effect of wet

424   deposition was weak. In addition, the corresponding low T and high RH stimulated the formation of

425   NO_3^- from gaseous state (HNO_3). On the O_3PD, the MLH was approximately 1300 m, and the NOR

426   turned to decrease, demonstrating a more significant role of the partitioning process between gas and

427   aerosols than that of the atmospheric oxidation process at this stage. On the NPD, the MLH was the

428   highest, with a value of approximately 2400 m, and the $PM_{2.5}$ chemical composition was dominated by

429   OM.

430   To explore the relevance of hourly O_3, $PM_{2.5}$, its components, and MLH, we have taken PuY and

431   HeZ as examples. Figure S4 plotted the day-to-day variations along with the diurnal variations in O_3,

432    $PM_{2.5}$, its components, and MLH in PuY and HeZ during Episode II (June 18−29, 2021). The results

433 showed that there was large diurnal and day-to-day variability in O_3 and $PM_{2.5}$ levels. Diurnal

434 variations in MLH were clearly visible (Figure S5), with an increase in MLH during the daytime and a

435 decrease at night. The concentration of $PM_{2.5}$ increased with the decrease in MLH at night, but the

436 concentration of O_3 increased with an increase in MLH during the daytime. Interestingly, we observed

437 noontime soar of SO_4^{2-} and OC concentrations in PuY, and the values of SOR remained stable or even

438 increased at noon. Additionally, O_3 and $PM_{2.5}$ gradually accumulated with the development of mixing

439 layer during June 18−21 and 26−28, which can be attributed to the O_3 and $PM_{2.5}$

440 superposition-composite effects. The decrease in $PM_{2.5}$ during the daytime with the rise in MLH, can

441 be offset partly by an increment in secondary pollutant formation derived from O_3 growth. Then, with

442 the decrease in MLH at night, the concentration of the original existing $PM_{2.5}$ increased owing to

443 unfavourable diffusion. In general, the conclusions of this study are only suitable for the day-to-day

444 relationship between air pollutants and MLH. Hourly relationships are much more complicated and

445 require further analysis.

446
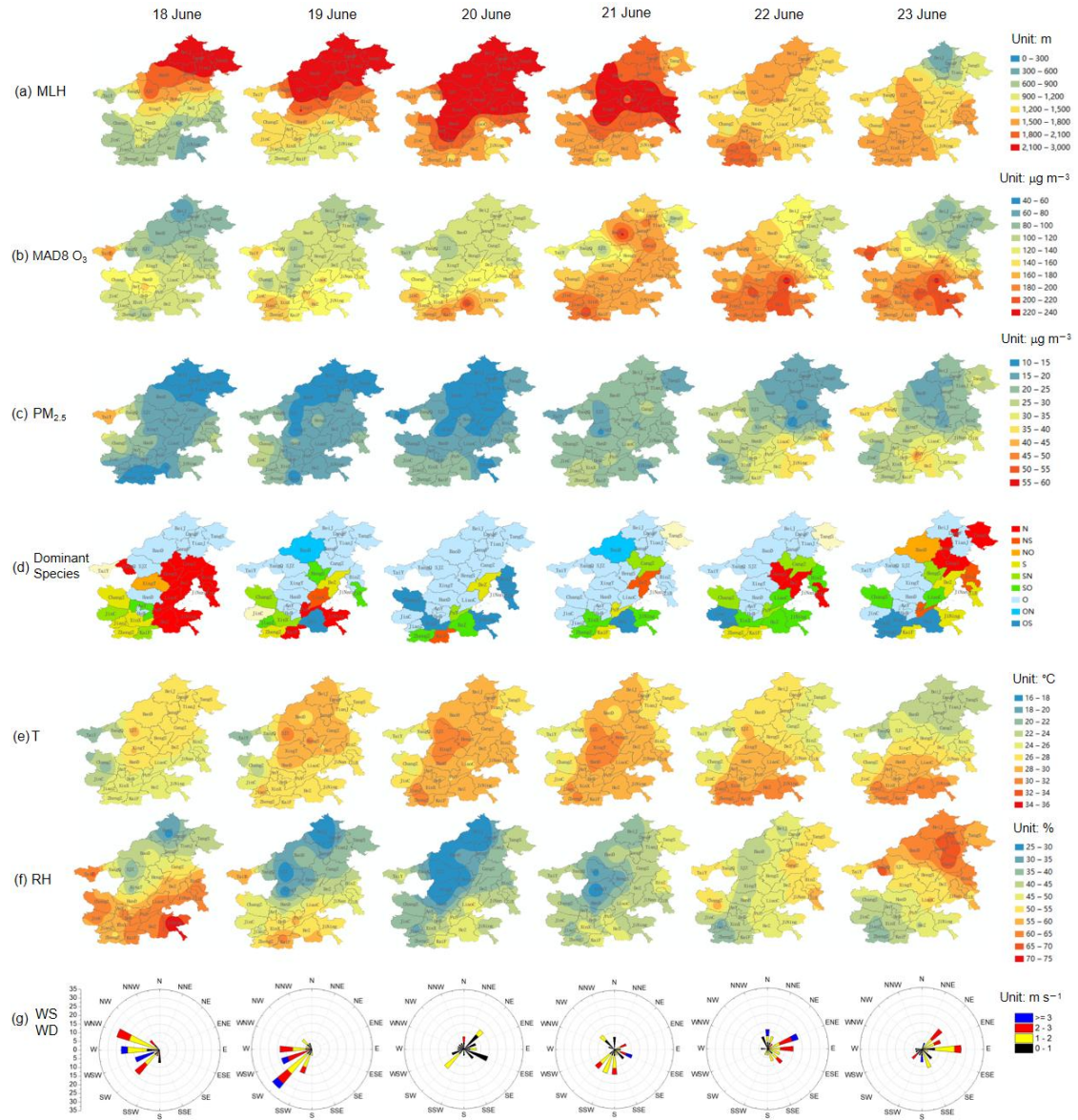
Figure 9. Spatial distribution of (a) MLH, (b) MDA8 O_3, (c) $PM_{2.5}$, (d) the dominant $PM_{2.5}$ chemical component (N: NO_3^- dominant, NS: NO_3^- and SO_4^{2-} dominant, NO: NO_3^- and OM dominant, S: SO_4^{2-} dominant, SN: SO_4^{2-} and NO_3^- dominant, SO: SO_4^{2-} and OM dominant, O: OM dominant, ON: OM and NO_3^- dominant, OS: OM and SO_4^{2-} dominant), (e) T, and (f) RH, (g) the overall change characteristics of WS and WD in the NCP from June 18 to 23, 2021. The dominant $PM_{2.5}$ chemical component type was identified as the method proposed by Wang et al. (2022b): if the mass fraction of the maximum component was 1.2 times higher than that of the secondary one, the former was considered as the dominant factor, otherwise both dominated $PM_{2.5}$ formation.
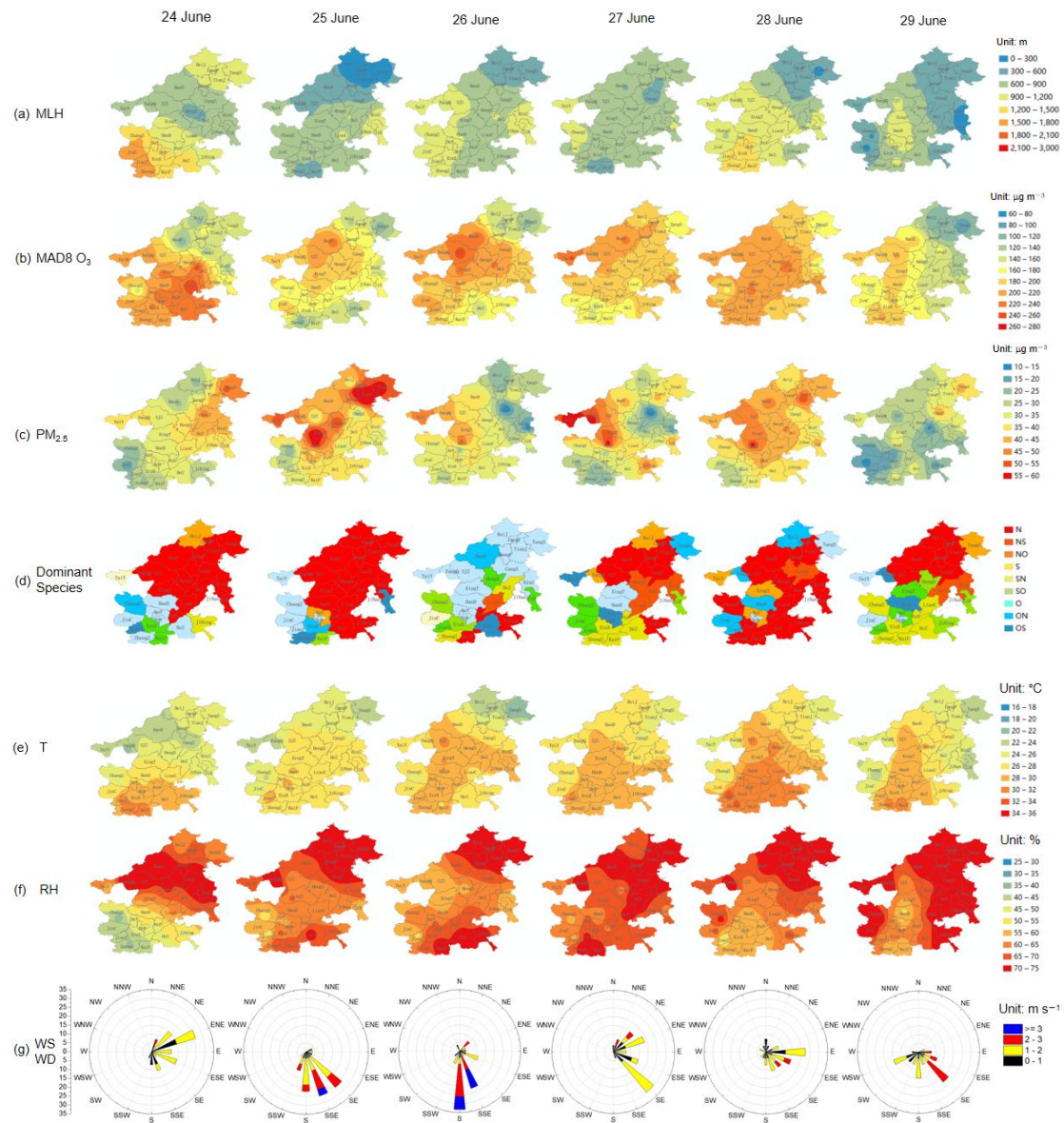
Figure 10. Spatial distribution of (a) MLH, (b) MDA8 O$_3$, (c) PM$_{2.5}$, (d) the dominant PM$_{2.5}$ chemical component (N: NO$_3^-$ dominant, NS: NO$_3^-$ and SO$_4^{2-}$ dominant, NO: NO$_3^-$ and OM dominant, S: SO$_4^{2-}$ dominant, SN: SO$_4^{2-}$ and NO$_3^-$ dominant, SO: SO$_4^{2-}$ and OM dominant, O: OM dominant, ON: OM and NO$_3^-$ dominant, OS: OM and SO$_4^{2-}$ dominant), (e) T, and (f) RH, (g) the overall change characteristics of WS and WD in the NCP from June 24 to 29, 2021. The dominant PM$_{2.5}$ chemical component type was identified as the method proposed by Wang et al. (2022b): if the mass fraction of the maximum component was 1.2 times higher than that of the secondary one, the former was considered as the dominant factor, otherwise both dominated PM$_{2.5}$ formation.
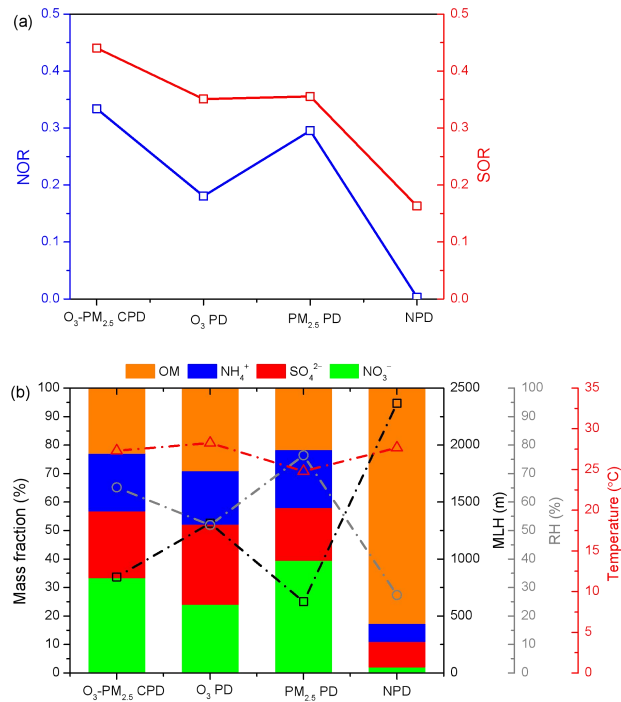
467

468 **Figure 11.** Distribution characteristics of (a) NOR and SOR, and (b) the mass fractions of major PM$_{2.5}$

469 components, MLH, RH, and temperature under O$_3$–PM$_{2.5}$ CPD, O$_3$ PD, PM$_{2.5}$ PD, and NPD conditions

470 from June 24 to 29, 2021.

471 **3.4.2 Interaction between PM$_{2.5}$ and O$_3$ along with the evolution of MLH**

472
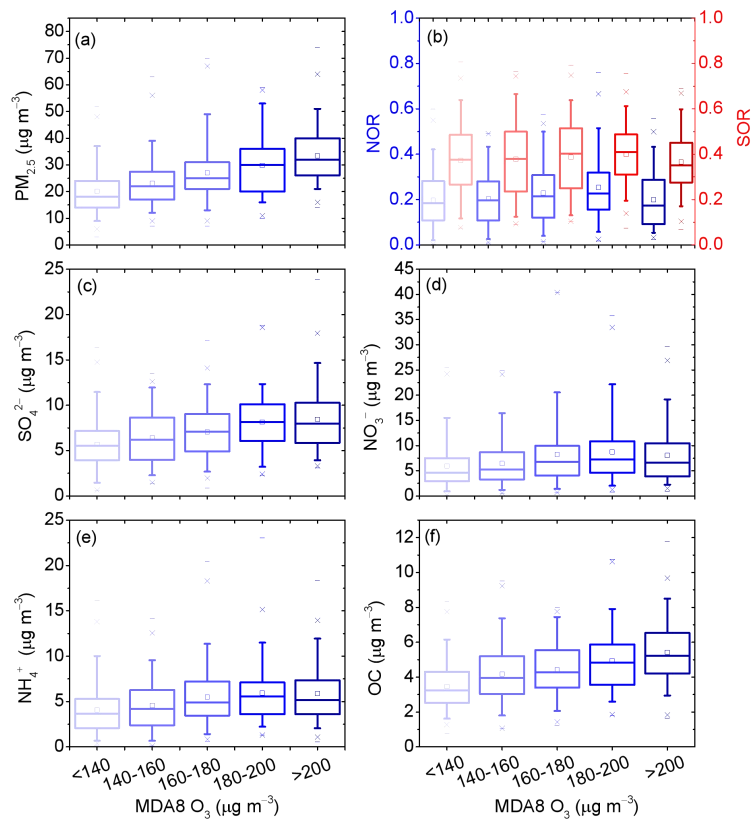
Figure 12. Box plots showing the statistics of (a) $PM_{2.5}$, (b) NOR and SOR, (c) SO_4^{2-}, (d) NO_3^-, (e) NH_4^+, and (f) OC for different MDA8 O_3 conditions (< 140, 140–160, 160–180, 180–200, and > 200 $\mu g \ m^{-3}$). The distance between the bottom and the top of the box reflects the inter quartile range; the line and square in between are the median and mean values, respectively. The whiskers above and below the box refer the 95 % confidence interval of the data. Note that rainy days were excluded.

Figure 12 displays the box-and-whisker plots of $PM_{2.5}$ and its major components for different MDA8 O_3 conditions. To isolate the impacts of precipitation on $PM_{2.5}$ concentration, these rainy days when the daily rainfall amount greater than 0 mm were excluded. Here the concentrations of $PM_{2.5}$ and its major components were found to increase synchronously with elevated MDA8 O_3 concentration, especially when MDA8 O_3 increased from < 140 to 180–200 $\mu g \ m^{-3}$. This summertime collaborative growth process of $PM_{2.5}$-O_3 has also been observed in other studies (Wang et al., 2022a; Wu et al., 2022). With elevated MDA8 O_3 concentration, SOR and NOR both slightly increased, and reached the maximum when MDA8 O_3 at around 160–200 $\mu g \ m^{-3}$, which indicated the strong secondary formation of SO_4^{2-} and NO_3^- promoted by high O_3 concentration. When MDA8 O_3 increased from 180–200 to > 200 $\mu g \ m^{-3}$, the concentrations of NO_3^-, NH_4^+, and SO_4^{2-} kept stable or began to decrease, and the values of SOR and NOR decreased synchronously. During this stage, the high O_3 concentration often accompanied by dry and hot meteorological conditions, which was not beneficial to aqueous chemical production and was conducive to the partitioning of nitrate to the gas phase.

To verify the potential impact of photochemical oxidation to the increase of $PM_{2.5}$ concentration with mixing layer development, the changes in $PM_{2.5}$ and MDA8 O_3 along with the increase of MLH were quantified in the "2+26" cities in the NCP. Linear regression equations between air pollutants and MLH were fitted during the initial increasing stage (300 m < MLH < 1200 m) and their slopes were shown in Figure 13. The slopes indicated the rates of the maximum changes in air pollutant concentration per unit change in the MLH (100 m). The slopes of $PM_{2.5}$ and O_3 were expressed as $\Delta PM_{2.5}$ and ΔO_3 ($\mu g \ m^{-3}$ (100) m^{-1}). It was found that $\Delta PM_{2.5}$ was closely related to ΔO_3 (R^2=0.58), and spatial difference in $\Delta PM_{2.5}$ and ΔO_3 was witnessed in the NCP during the observation period. $\Delta PM_{2.5}$ and ΔO_3 both showed high values in YangQ, , LangF and CangZ, with values of 7.56 and 20.24 $\mu g \ m^{-3}$ (100) m^{-1} in YangQ, 5.75 and 18.97 $\mu g \ m^{-3}$ (100) m^{-1} in LangF, and 4.02 and 19.49 $\mu g \ m^{-3}$ (100) m^{-1} in CangZ, respectively. Comparing with these cities, $\Delta PM_{2.5}$ and ΔO_3 were lowest in HeB, with the value of 3.54 and −2.02 $\mu g \ m^{-3}$ (100) m^{-1}, respectively, which implied that the secondary formation here was

weak and the surface PM$_{2.5}$ change characteristic was dominantly controlled by local emissions or vertical diffusion effect.

Compared to winter, photochemistry in summer is quite active because of strong solar radiation. Although a deep MLH favors the dilution of air pollutants, a higher MLH can also promote secondary chemical feedback by enhancing the availability of atmospheric oxidation capacity (such as changes in O$_3$) along with appropriate meteorological conditions. This conclusion corresponds well with the findings based on the chemical transport model (Dai et al., 2023), which proposed strong chemical production of secondary aerosols when the planetary boundary layer height was approximately 946.1m on O$_3$–PM$_{2.5}$ co-pollution days. The strong chemical productions in the oxidative atmosphere at medium MLH condition may overcome the dilution effect on PM$_{2.5}$ induced by mixing layer development, leading to higher PM$_{2.5}$ level at the ground level. However, it should be noted that the conclusions of this study are only suitable for summertime regional observations, especially for warm and humid season. Conditions were different in winter (much lower O$_3$ levels). More extended observations in time and space are needed in the future to further examine and better understand the complex interactions between MLH, air pollution, and chemical processing.
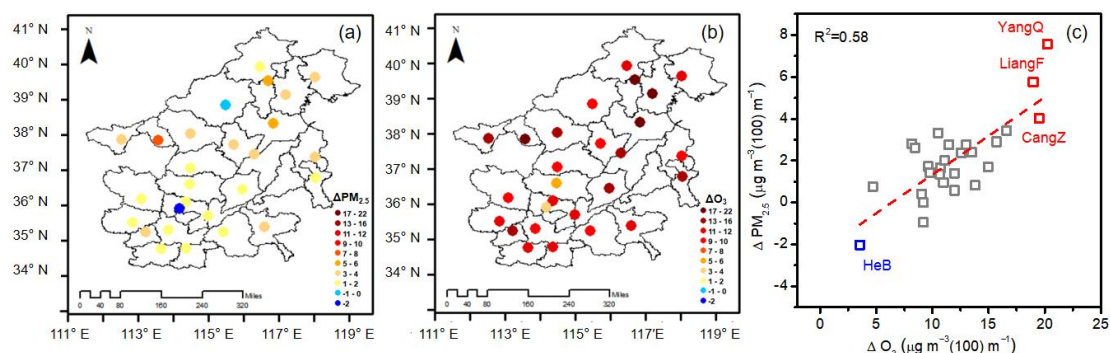
Figure 13. Spatial distribution of (a) ΔPM$_{2.5}$ and (b) ΔO$_3$. (c) The relationships between ΔPM$_{2.5}$ and ΔO$_3$ in the NCP during summertime. The corresponding correlation coefficients (R^2) was given at the top of the panel.

4 Conclusions

The MLH is generally considered as a critical physical parameter in atmospheric environmental evaluation. It is assumed that an extended mixing layer may lead to the dilution of air pollutants and thus tend to decrease surface concentrations. Several publications have indeed reported such

anti-correlations in cold seasons. However, the understanding of the interaction between near surface O_3 and $PM_{2.5}$ (including its major components) along with the evolution of the mixing layer during warm season, remains poor. Furthermore, previous observational studies were mostly limited to specific cities. This paper is devoted to these topics by examining the response of MDA8 O_3, $PM_{2.5}$, and its major components to the changes in mixing layer meteorology in the NCP during summer. We showed that MDA8 O_3 initially increased and then decreased with the growth of MLH. The maximum turning point of the MLH was approximately 900–1800 m. As for near-ground $PM_{2.5}$, a similar non-linear change profile was found, with the maximum value of 31.65 μg m^{-3} under medium MLH condition (900–1200 m), which was quite different from the results conducted in cold season. Compared to winter, the occurrence of low MLH during summer in the NCP was mostly accompanied by cloudy or rainy conditions, which promoted wet deposition and led to low concentrations of $PM_{2.5}$ at the ground level. Under medium MLH condition, strong chemical productions of SO_4^{2-} and OC occurred along with appropriate mixing layer meteorology, where RH was around 50−70 %, and the availability of atmospheric oxidants (i.e., O_3) increased. Strong chemical productions under medium MLH conditions may offset the diffusion effect on $PM_{2.5}$ induced by the mixing layer development, resulting in higher $PM_{2.5}$. The chemical characteristics of $PM_{2.5}$ changed significantly with the growth of MLH. The composited concentration of NO_3^- was the highest under low MLH condition, while the composited concentrations of SO_4^{2-} and OC increased under medium MLH condition. Temperature was the key factor controlling the different changes in NO_3^- and SO_4^{2-} concentrations in $PM_{2.5}$. We conclude that MLH can be an indicator of air pollutants in cold seasons, but the correlation between MLH and air pollutants, such as O_3 and $PM_{2.5}$, should be treated with care during hot season. At least for the observation period in the NCP this was not the case. Although several studies have examined the change characteristics of the MLH and its influence on ground-level O_3 and $PM_{2.5}$, it remains challenging to elucidate the mechanisms underlying these complex relationships. In this study, we did not quantify the sensitivity of O_3 and $PM_{2.5}$ to different meteorological factors and chemical processes. To better understand the complex interactions among MLH, air pollution, and chemical processing, a more detailed consideration of the aids of explicit models should be needed in the future. We also note that the present study is only confined to summer conditions (including two summer months) in the NCP, and the conclusions are likely to differ for other seasons and regions. Therefore, more extensive observations in time and space are required in the future.

556

Data availability. The data used in this paper can be provided upon request from the corresponding author.

Author contributions. J W, J G and H L conceived the study and designed the experiments. **J W, F C, X Y,Y Y, L L and Y X** analyzed the data. **J W** prepared the manuscript and all the coauthors helped improve the manuscript.

Competing interests. The authors declare that they have no conflict of interest.

Acknowledgement. We thank the platform of National Atmospheric Particulate Chemical-Speciation-Network for making the $PM_{2.5}$ chemical composition data available.

Financial support. This work was supported by the National Natural Science Foundation of China (No. 42075182), the National research program for key issues in air pollution control (DQGG2021101) and the Central Level, Scientific Research Institutes for Basic R&D Special Fund Business, China (No. 2022YSKY-26).

573   **Reference**

574   Cheng, J., Su, J., Cui, T., Li, X., Dong, X., Sun, F., Yang, Y., Tong, D., Zheng, Y., Li, Y., Li, J., Zhang,

575   Q., and He, K.: Dominant role of emission reduction in $PM_{2.5}$ air quality improvement in Beijing

576   during 2013–2017: a model-based decomposition analysis, Atmos. Chem. Phys., 19, 6125-6146,

577   10.5194/acp-19-6125-2019, 2019.

578   Chow, W. S., Liao, K., Huang, X. H. H., Leung, K. F., Lau, A. K. H., and Yu, J. Z.: Measurement report:

579   The 10-year trend of $PM_{2.5}$ major components and source tracers from 2008 to 2017 in an urban site

580   of Hong Kong, China, Atmos. Chem. Phys., 22, 11557-11577, 10.5194/acp-22-11557-2022, 2022.

581   Chu, B., Ma, Q., Liu, J., Ma, J., Zhang, P., Chen, T., Feng, Q., Wang, C., Yang, N., Ma, H., Ma, J.,

582   Russell, A. G., and He, H.: Air Pollutant Correlations in China: Secondary Air Pollutant Responses

583   to NOx and SO_2 Control, Environ. Sci. Technol. Let., 7, 695-700, 10.1021/acs.estlett.0c00403, 2020.

584   Cohen, A. J., Brauer, M., Burnett, R., Anderson, H. R., Frostad, J., Estep, K., Balakrishnan, K.,

585   Brunekreef, B., Dandona, L., and Dandona, R.: Estimates and 25-year trends of the global burden of

586   disease attributable to ambient air pollution: an analysis of data from the Global Burden of Diseases

587   Study 2015, Lancet, 2017.

588   Dai, H., Liao, H., Li, K., Yue, X., Yang, Y., Zhu, J., Jin, J., Li, B., and Jiang, X.: Composited analyses

589   of the chemical and physical characteristics of co-polluted days by ozone and $PM_{2.5}$ over 2013–2020

590   in the Beijing–Tianjin–Hebei region, Atmos. Chem. Phys., 23, 23-39, 10.5194/acp-23-23-2023,

591   2023.

592   Dang, R., Liao, H., and Fu, Y.: Quantifying the anthropogenic and meteorological influences on

593   summertime surface ozone in China over 2012–2017, Sci. Total. Environ., 754, 142394,

594   10.1016/j.scitotenv.2020.142394, 2021.

595   Dawson, J. P., Adams, P. J., and Pandis, S. N.: Sensitivity of $PM_{2.5}$ to climate in the Eastern US: a

596   modeling case study, Atmos. Chem. Phys., 7, 4295-4309, 10.5194/acp-7-4295-2007, 2007.

597   Dian, J., Seidel, Chi, O., Ao, and, Kun, and Li: Estimating climatological planetary boundary layer

598   heights from radiosonde observations: Comparison of methods and uncertainty analysis, J. Geophys.

599   Res. Atmos., 10.1029/2009JD013680, 2010.

600   Du, C., Liu, S., Yu, X., Li, X., Chen, C., Peng, Y., Dong, Y., Dong, Z., and Wang, F.: Urban boundary

601   layer height characteristics and relationship with particulate matter mass concentrations in Xi'an,

602   Central China, Aerosol Air Qual. Res., 13, 1598-1607, 10.4209/aaqr.2012.10.0274, 2013.

603   Gao, Y. and Ji, H.: Microscopic morphology and seasonal variation of health effect arising from heavy

604   metals in $PM_{2.5}$ and PM_{10}: One-year measurement in a densely populated area of urban Beijing,

605   Atmos. Res., 212, 213-226, https://doi.org/10.1016/j.atmosres.2018.04.027, 2018.

606   Geiß, A., Wiegner, M., Bonn, B., Schäfer, K., Forkel, R., von Schneidemesser, E., Münkel, C., Chan, K.

607   L., and Nothard, R.: Mixing layer height as an indicator for urban air quality?, Atmos. Meas. Tech.,

608   10.5194/amt-2017-53, 2017.

609   Haman, C. L., Couzo, E., Flynn, J. H., Vizuete, W., Heffron, B., and Lefer, B. L.: Relationship between

610   boundary layer heights and growth rates with ground-level ozone in Houston, Texas, J. Geophys. Res.

611   Atmos., 119, 6230-6245, 10.1002/2013jd020473, 2014.

612   Haugen, D. A., Kaimal, J. C., Bradley, E. F.: An experimental study of Reynolds stress and heat flux in

613   the atmospheric surface layer, Q. J. Roy. Meteor. Soc., 97, 168-180, 1971.

614   Hou, P. and Wu, S.: Long-term changes in extreme air pollution meteorology and the implications for

615   air quality, Sci. Rep., 6, 23792, 10.1038/srep23792, 2016.

616   Jiang, N., Li, L., Wang, S., Li, Q., Dong, Z., Duan, S., Zhang, R., and Li, S.: Variation tendency of

617   pollution characterization, sources, and health risks of $PM_{2.5}$-bound polycyclic aromatic

618   hydrocarbons in an emerging megacity in China: Based on three-year data, Atmos. Res., 217, 81-92,

619   2018.

620   Kang, M., Zhang, J., Zhang, H., and Ying, Q.: On the relevancy of observed ozone increase during

621   COVID-19 lockdown to summertime ozone and $PM_{2.5}$ control policies in China, Environ. Sci.

622   Technol. Let., 8, 289-294, 10.1021/acs.estlett.1c00036, 2021.

623   Kong, L., Du, C., Zhanzakova, A., Cheng, T., and Zhang, S.: Trends in heterogeneous aqueous reaction

624   in continuous haze episodes in suburban Shanghai: An in-depth case study, Sci. Total Environ., 634,

625   1192, 10.1016/j.scitotenv.2018.04.086, 2018.

626   Li, J., Cai, J., Zhang, M., Liu, H., Han, X., Cai, X., and Xu, Y.: Model analysis of meteorology and

627   emission impacts on springtime surface ozone in Shandong, Sci. Total. Environ., 771, 144784,

628   https://doi.org/10.1016/j.scitotenv.2020.144784, 2021.

629   Liu, J., Wu, D., Fan, S., Mao, X., and Chen, H.: A one-year, on-line, multi-site observational study on

630   water-soluble inorganic ions in $PM_{2.5}$ over the Pearl River Delta region, China, Sci. Total Environ.,

631   601-602, 1720-1732, https://doi.org/10.1016/j.scitotenv.2017.06.039, 2017a.

Liu, P., Ye, C., Xue, C., Zhang, C., Mu, Y., and Sun, X.: Formation mechanisms of atmospheric nitrate and sulfate during the winter haze pollution periods in Beijing: gas-phase, heterogeneous and aqueous-phase chemistry, Atmos. Chem. Phys., 20, 4153-4165, 10.5194/acp-20-4153-2020, 2020.

Liu, T., Gong, S., He, J., Yu, M., and Zhao, Q.: Attributions of meteorological and emission factors to the 2015 winter severe haze pollution episodes in China's Jing-Jin-Ji area, Atmos. Chem. Phys., 17, 2971-2980, 10.5194/acp-17-2971-2017, 2017b.

Lou, M., Guo, J., Wang, L., Xu, H., Chen, D., Miao, Y., Lv, Y., Li, Y., Guo, X., Ma, S., and Li, J.: On the relationship between aerosol and boundary layer height in summer in China under different thermodynamic conditions, Earth Space Sci., 6, 887-901, 10.1029/2019ea000620, 2019.

Lu, M., Tang, X., Wang, Z., Wu, L., Chen, X., Liang, S., Zhou, H., Wu, H., Hu, K., Shen, L., Yu, J., and Zhu, J.: Investigating the transport mechanism of $PM_{2.5}$ pollution during January 2014 in Wuhan, Central China, Adv. Atmos. Sci., 36, 1217-1234, 10.1007/s00376-019-8260-5, 2019.

Ma, S., Shao, M., Zhang, Y., Dai, Q., and Xie, M.: Sensitivity of $PM_{2.5}$ and O_3 pollution episodes to meteorological factors over the North China Plain, Sci. Total. Environ., 792, 148474, 10.1016/j.scitotenv.2021.148474, 2021.

Markovic, M. Z., VandenBoer, T. C., and Murphy, J. G.: Characterization and optimization of an online system for the simultaneous measurement of atmospheric water-soluble constituents in the gas and particle phases, J. Environ. Monit., 14, 1872-1884, 10.1039/c2em00004k, 2012.

Miao, Y., Che, H., Zhang, X., and Liu, S.: Relationship between summertime concurring $PM_{2.5}$ and O_3 pollution and boundary layer height differs between Beijing and Shanghai, China, Environ. Pollut., 268, 115775, 10.1016/j.envpol.2020.115775, 2021.

Murthy, B. S., Latha, R., Tiwari, A., Rathod, A., Singh, S., and Beig, G.: Impact of mixing layer height on air quality in winter, J. Atmos. Sol.-Terr. Phy., 197, 10.1016/j.jastp.2019.105157, 2020.

NASTRO (The North American Research Strategy for Tropospheric Ozone): An assessment of tropospheric ozone pollution: a North American perspective , 2000.

Niu, T., Wang, J., Yang, Y., Wang, Y., and Chen, C.: A study on parameterization of the Beijing winter heavy haze events associated with height of pollution mixing layer, Adv. Meteorol., 2017, 1-11, 10.1155/2017/8971236, 2017.

Pan, L., Xu, J., Tie, X., Mao, X., Gao, W., and Chang, L.: Long-term measurements of planetary boundary layer height and interactions with $PM_{2.5}$ in Shanghai, China, Atmos. Pollut. Res., 10,

989-996, 10.1016/j.apr.2019.01.007, 2019.

Pang, N., Gao, J., Che, F., Ma, T., Liu, S., Yang, Y., Zhao, P., Yuan, J., Liu, J., Xu, Z., and Chai, F.: Cause of $PM_{2.5}$ pollution during the 2016–2017 heating season in Beijing, Tianjin, and Langfang, China, J. Environ. Sci. (China), 95, 201-209, 10.1016/j.jes.2020.03.024, 2020.

Park, S. S., Jung, S. A., Gong, B. J., Cho, S. Y., and Lee, S. J.: Characteristics of $PM_{2.5}$ haze episodes revealed by highly time-resolved measurements at an air pollution monitoring supersite in Korea, Aerosol Air Qual. Res., 13, 957-976, 10.4209/aaqr.2012.07.0184, 2013.

Porter, W. C. and Heald, C. L.: The mechanisms and meteorological drivers of the summertime ozone–temperature relationship, Atmos. Chem. Phys., 19, 13367-13381, 10.5194/acp-19-13367-2019, 2019.

Reddy, K. K., Naja, M., Ojha, N., Mahesh, P., and Lal, S.: Influences of the boundary layer evolution on surface ozone variations at a tropical rural site in India, J. Earth Syst. Sci., 121, 911-922, 10.1007/s12040-012-0200-z, 2012.

Rumsey, I. C., Cowen, K. A., Walker, J. T., Kelly, T. J., Hanft, E. A., Mishoe, K., Rogers, C., Proost, R., Beachley, G. M., Lear, G., Frelink, T., and Otjes, R. P.: An assessment of the performance of the Monitor for AeRosols and GAses in ambient air (MARGA): a semi-continuous method for soluble compounds, Atmos. Chem. Phys., 14, 5639-5658, 10.5194/acp-14-5639-2014, 2014.

Seinfeld, J. H. and Pandis, S. N.: Atmospheric Chemistry and Physics: From Air Pollution to Climate Change, . 2nd ed.; J. Wiley: Hoboken, N.J.,, p xxviii, 1203 p., 2006.

Steiner, Allison, L., Davis, Adam, J., Sillman, Sanford, Owen, Robert, C., Michalak, and Anna, M.: Observed suppression of ozone formation at extremely high temperatures due to chemical and biophysical feedbacks Proc. Natl. Acad. Sci. U. S. A., 107, 19685–19690, 2010.

Stull, R.: An Introduction to Boundary Layer Meteorology, Kluwer Academic Publishers, Dordrecht, the Netherlands, 1988.

Wang, F., Wang, W., Wang, Z., Zhang, Z., Feng, Y., Russell, A. G., and Shi, G.: Drivers of $PM_{2.5}$−O_3 co-pollution: from the perspective of reactive nitrogen conversion pathways in atmospheric nitrogen cycling, Sci. Bull. (Beijing), 67, 1833-1836, 10.1016/j.scib.2022.08.016, 2022a.

Wang, J., Bian, L., Xiao, C.: Dynamics of ekman boundary layer over the antarctic plateau in summer, Chinese Sci. Bull., 59, 999–1005, 2014.

Wang, J., Yang, Y.: Modern weather engineering. Meteorological Press, Beijing, 334–339, 2000.

Wang, J., Yang, Y., Zhang, X., Liu, H., Che, H., Shen, X., and Wang, Y.: On the influence of atmospheric super-saturation layer on China's heavy haze-fog events, Atmos. Environ., 171, 261-271, https://doi.org/10.1016/j.atmosenv.2017.10.034, 2017.

Wang, J., Gao, J., Che, F., Wang, Y., Lin, P., and Zhang, Y.: Dramatic changes in aerosol composition during the 2016–2020 heating seasons in Beijing–Tianjin–Hebei region and its surrounding areas: The role of primary pollutants and secondary aerosol formation, Sci. Total. Environ., 849, 157621, 10.1016/j.scitotenv.2022.157621, 2022b.

Wang, J., Yang, Y., Jiang, X., Wang, D., Zhong, J., and Wang, Y.: Observational study of the $PM_{2.5}$ and O_3 superposition-composite pollution event during spring 2020 in Beijing associated with the water vapor conveyor belt in the northern hemisphere, Atmos. Environ., 272, 10.1016/j.atmosenv.2022.118966, 2022c.

Wang, M., Duan, Y., Xu, W., Wang, Q., Zhang, Z., Yuan, Q., Li, X., Han, S., Tong, H., Huo, J., Chen, J., Gao, S., Wu, Z., Cui, L., Huang, Y., Xiu, G., Cao, J., Fu, Q., and Lee, S.-c.: Measurement report: Characterisation and sources of the secondary organic carbon in a Chinese megacity over 5 years from 2016 to 2020, Atmos. Chem. Phys., 22, 12789-12802, 10.5194/acp-22-12789-2022, 2022d.

Wang, X., Xiang, Y., Liu, W., Lv, L., Dong, Y., Fan, G., Ou, J., and Zhang, T.: Vertical profiles and regional transport of ozone and aerosols in the Yangtze River Delta during the 2016 G20 summit based on multiple lidars, Atmos. Environ., 259, 10.1016/j.atmosenv.2021.118506, 2021.

Wen, L., Xue, L., Wang, X., Xu, C., Chen, T., Yang, L., Wang, T., Zhang, Q., and Wang, W.: Summertime fine particulate nitrate pollution in the North China Plain: increasing trends, formation mechanisms and implications for control policy, Atmos. Chem. Phys., 18, 11261-11275, 10.5194/acp-18-11261-2018, 2018.

World Health Organization. WHO global air quality guidelines: particulate matter ($PM_{2.5}$ and PM_{10}), ozone, nitrogen dioxide, sulfur dioxide and carbon monoxide. Geneva: World Health Organization, 2021.

Wu, W. and Wang, T.: On the performance of a semi-continuous $PM_{2.5}$ sulphate and nitrate instrument under high loadings of particulate and sulphur dioxide, Atmos. Environ., 41, 5442-5451, https://doi.org/10.1016/j.atmosenv.2007.02.025, 2007.

Wu, X., Xin, J., Zhang, W., Gao, W., Ma, Y., Ma, Y., Wen, T., Liu, Z., Hu, B., Wang, Y., and Wang, L.: Variation characteristics of air combined pollution in Beijing City, Atmos. Res., 274,

722   10.1016/j.atmosres.2022.106197, 2022.

723   Xu, X., Zhang, H., Lin, W., Wang, Y., Xu, W., and Jia, S.: First simultaneous measurements of

724   peroxyacetyl nitrate (PAN) and ozone at Nam Co in the central Tibetan Plateau: impacts from the

725   PBL evolution and transport processes, Atmos. Chem. Phys., 18, 5199-5217,

726   10.5194/acp-18-5199-2018, 2018.

727   Yu, S.: Fog geoengineering to abate local ozone pollution at ground level by enhancing air moisture,

728   Environ. Chem. Lett., 17, 565-580, 10.1007/s10311-018-0809-5, 2019.

729   Zhang, G., Bian, L., Wang, J., Yang, Y., Yao, W., Xu, X.: The boundary layer characteristics in the

730   heavy fog formation process over Beijing and its adjacent areas, Sci. China Earth Sci., 48, 88–101,

731   2005.

732   Zhang, H., Wang, Y., Hu, J., Ying, Q., and Hu, X.-M.: Relationships between meteorological

733   parameters and criteria air pollutants in three megacities in China, Environmental Research, 140,

734   242-254, https://doi.org/10.1016/j.envres.2015.04.004, 2015a.

735   Zhang, R., Wang, G., Guo, S., Zamora, M. L., Ying, Q., Lin, Y., Wang, W., Hu, M., and Wang, Y.:

736   Formation of urban fine particulate matter, Chem. Rev., 115, 3803-3855,

737   10.1021/acs.chemrev.5b00067, 2015b.

738   Zhang, X., Xiao, X., Wang, F., Brasseur, G., Chen, S., Wang, J., and Gao, M.: Observed sensitivities of

739    $PM_{2.5}$ and O_3 extremes to meteorological conditions in China and implications for the future,

740   Environ. Int., 168, 107428, 10.1016/j.envint.2022.107428, 2022.

741   Zhao, W., Tang, G., Yu, H., Yang, Y., Wang, Y., Wang, L., An, J., Gao, W., Hu, B., Cheng, M., An, X.,

742   Li, X., and Wang, Y.: Evolution of boundary layer ozone in Shijiazhuang, a suburban site on the

743   North China Plain, J. Environ. Sci. (China), 83, 152-160, 10.1016/j.jes.2019.02.016, 2019.

744   Zhu, X., Tang, G., Guo, J., Hu, B., Song, T., Wang, L., Xin, J., Gao, W., Münkel, C., Schäfer, K., Li, X.,

745   and Wang, Y.: Mixing layer height on the North China Plain and meteorological evidence of serious

746   air pollution in southern Hebei, Atmos. Chem. Phys., 18, 4897-4910, 10.5194/acp-18-4897-2018,

747   2018.

748